NASA TN D-105

TECHNICAL NOTE
D-105

AN ANALOG STUDY OF AN AIRBORNE AUTOMATIC LANDING-APPROACH SYSTEM

By James J. Adams

Langley Research Center
Langley Field, Va.

NATIONAL AERONAUTICS AND SPACE ADMINISTRATION

WASHINGTON

December 1959

NATIONAL AERONAUTICS AND SPACE ADMINISTRATION

TECHNICAL NOTE D-105

AN ANALOG STUDY OF AN AIRBORNE AUTOMATIC LANDING-APPROACH SYSTEM

By James J. Adams

SUMMARY

Analysis indicates that it is possible to control an airplane in a landing-approach maneuver by means of an automatic control scheme which derives its error signals from airborne attitude-measuring equipment and airborne radar equipment tracking a target located at the end of the runway. An analog study has been made of such a system. A swept-wing jet fighter airplane was represented by six-degree-of-freedom equations with linear aerodynamic coefficients. The radar and attitude information was assumed to be free of any lag or dynamics. The control system using these radar and attitude measurements appears to be feasible. To a certain extent the details of the system were also investigated. Factors such as various initial conditions, disturbances such as flap deflection, gust disturbances, and radar noise were investigated.

An idea of the maximum gains relating control-surface deflection to error signals that can be used is illustrated by the example used in the investigation. It was also shown that the attitude measurements needed to define the displacement errors must be measurements of Euler angles rather than the integral of body axes rotations. An instability was indicated under the circumstances of extremely large longitudinal error at short range, and a possible remedy was investigated.

INTRODUCTION

Approach systems that are presently in use, such as ILS and AGCA systems, require complex equipment on the ground. In contrast to these systems, an automatic approach system may be devised using a simple radar target on the ground and the radar tracking set and attitude-measuring equipment in the airplane. The simplicity of the ground equipment required in such a scheme could, in itself, be a worthwhile advantage in providing bad-weather facilities for an airfield. In addition, such a system has the advantage of allowing the complex parts of the system to be adjusted to match the individual characteristics of the airplane carrying this equipment.

An analog study has been made to determine the feasibility of a control system using perfect signals from the airborne equipment. To a certain extent the details of the system are also investigated so that the results may be evaluated and compared with other systems.

DESCRIPTION

General

This analysis deals with the problem of controlling an airplane to the landing-approach glide-slope center line using airborne equipment. Only the straight-line part of the approach is considered. The final flare and touchdown is not considered in this analysis. The airplane was assumed to be equipped with a tracking radar or similar target-seeking equipment capable of establishing the line of sight between the airplane and a target located at or near the approach end of the runway, and attitude gyros which can measure the pitch, roll, and direction angles of the airplane. An outline of the complete system is given in the block diagram of figure 1. (Symbols are defined in appendix A.) As is shown in the figure, it was assumed that the rudder, ailerons, throttle, and elevator controls would be used to control the airplane, and that various outputs of the airplane, attitude gyros, and radar, would be used to position these controls.

Error Signals

The lateral and longitudinal error signals, or outer-loop signals, were obtained in the following manner. The lateral error signal was obtained by adding the radar deflection angle θ_a to the Euler yaw angle ψ_{eu}. The geometry of this situation is shown in figure 2. In operational procedure it was assumed that the magnetic heading of the runway would be added to the output of the directional gyro as a bias signal, so that the directional-gyro output would be a measure of the deviation of the heading of the airplane from the center line of the runway. The lateral error can be thought of as the angle between the center line and a line drawn from the end of the runway to the airplane. Similarly, the longitudinal error signal is the sum of the radar elevation angle θ_e, the Euler pitch angle θ_{eu}, and a $2\frac{1}{2}^\circ$ bias signal. This bias signal is added to the longitudinal error signal so that the airplane will be controlled to a $2\frac{1}{2}^\circ$ glide slope. In operational procedure it is assumed that the airplane will be flying level when the approach control is turned on, and the airplane pitch angle that exists at that time will be referred to as the zero pitch angle. The airplane will then be controlled to

a flight-path angle $2\frac{1}{2}^{\circ}$ below the initial flight path. The longitudinal error signal is, then, the angle between a $2\frac{1}{2}^{\circ}$ glide slope and a line drawn from the end of the runway to the airplane, as is shown in figure 2.

As the basic philosophy of the approach system, it was assumed that these error signals would command changes in bank angle and pitch angle. The commanded bank angle and the accompanying change in horizontal force would tend to reduce the lateral error, and the change in pitch angle, with the accompanying change in direction of the forward velocity vector, would tend to reduce the longitudinal error. It was therefore necessary to add a bank-angle signal $\int p\,dt$ to the lateral error and a pitch-angle signal $\int q\,dt$ to the longitudinal error. A given lateral angular displacement would, therefore, result in a proportional bank-angle change, and a given vertical angular displacement would result in a proportional pitch-angle change.

Damping

The use of the error signals described above would result in an undamped motion in the mode representing the position of the airplane with respect to the glide-slope center line, similar to the motion of a spring-mass system. Fortunately, a suitable damping signal is readily available. Since the Euler heading angle is proportional to the rate of change of the position of the airplane with respect to the center line, this variable can be used to damp the lateral mode of motion. Similarly, the Euler pitch angle can be used to damp the longitudinal motion.

One specific purpose of the investigation was to determine the maximum gains that could be used on the error signals. It is desirable that these gains be as large as possible to insure precise control to the glide-slope center line in the presence of external disturbances. It is also desirable to adjust the ratio of the error signal to the damping signal to insure a rapid response with suitable damping. However, these signals which damp the mode of motion which describes the position of the airplane with respect to the glide-slope center line are also attitude signals with respect to the airplane alone and can directly affect the short-period characteristics. Their allowable magnitude therefore depends on the dynamics of the airplane.

Airplane and Autopilot

The airplane was assumed to be a swept-wing fighter airplane, and was simulated by six-degree-of-freedom equations with linear aerodynamic coefficients. The gravity terms were included in these equations as functions of Euler angles. All of the symbols and equations used are listed in appendixes A and B. The dynamic characteristics of the uncoupled longitudinal and lateral modes of motion are given in table I. It was assumed that the type of airplane chosen for the example would very likely have some yaw and pitch damping augmentation to insure desirable damping. Those damping additions together with the roll-attitude and pitch-attitude control might be thought of as representing a typical attitude autopilot. The characteristics of the airplane in combination with these typical autopilot loops were kept constant throughout the investigations. The dynamic characteristics of the airplane-autopilot are listed in table I also. Perfect control servos were assumed throughout the investigation.

L
4
9
3

Airspeed Control

In order for the longitudinal error signal to operate in the manner described before, it is necessary that the airspeed be kept constant. Therefore it was assumed that the throttle control was operated as a function of Euler pitch angle so that the change in thrust would approximately cancel the change in gravity force along the longitudinal body axis. The thrust expression used in the equations included a first-order lag term with a 1-second time constant. Experiments have shown that this is a good representation for the thrust response of a jet engine when changes of the order of 20 percent of total revolutions per minute are called for. It is estimated that the approximate change in revolutions per minute that will be called for in this problem is within this range. In addition to the pitch-angle signal, an airspeed signal was added to the throttle control. The gain used for the airspeed feedback was -68 lb/ft/sec.

Nonlinearity of Error Signals

It should be noted that the description given before for the outer-loop error signals and presented in figure 2 is true only when the wings of the airplane are level. The angles that are described by the error signals have no simple physical interpretation when the airplane is banked. The exact mathematical expressions for the perfect radar angles are as follows:

$$\theta_a = \theta_{a,o} + \int \left[\Omega_{Z_r} \sec \theta_e - r - \left(q \sin \theta_a + p \cos \theta_a\right)\tan \theta_e\right] dt \qquad (1)$$

$$\theta_e = \theta_{e,o} + \int \left(\Omega_{Y_r} - q \cos \theta_a + p \sin \theta_a\right) dt \qquad (2)$$

A pictorial definition of the radar angles together with a sketch of the radar gimbal arrangement is given in figure 3.

The fundamental purpose of this investigation was to determine if the error signals, which are a function of the radar angles, could be used to command an airplane to a glide-slope center line during maneuvers that would cause changes to occur in all of the variables involved in equations (1) and (2).

It should be realized that if the radar rotation was expressed as component orthogonal angles in the initial earth-axis system, the error signals would satisfy the description given before for all airplane positions. That is to say, if the orientation of the line of sight with respect to the airplane were defined by two angles in the horizontal and vertical planes of the earth-axis system, these angles would not be affected by a change in bank angle of the airplane. Such earth orientated error signals were tried once with relatively low gains, and the indication was that they would be very satisfactory. However, to manufacture such space-system angles from the given radar angles would require the presence of a complex computer in the control system, and therefore that scheme was not examined in detail. This is in contrast to defining the orientation of the line of sight in the radar-axis system in which, for example, a deflection angle would be traded for an elevation angle when the airplane bank angle changed 90°. The simplicity of mechanizing the control system using the radar angles directly as measured makes it desirable to use such a scheme if it can be made to give satisfactory results.

One further thought concerns the angles measured by the directional and vertical gyros. It is assumed that these instruments are gimbaled to read Euler angles. A pictorial definition of Euler angles is given in figure 4. The gimbal arrangement for a standard vertical gyro is shown in figure 5(a). In this arrangement the gyro spin axis is vertical, and pitch angle is measured on the inner gimbal. The actual angle measured on this inner gimbal will deviate from the true Euler angle depending on the combination of bank and pitch angles that exists. Reference 1 shows the amount of deviation that will be experienced. These deviations will be large for pitch angles near 90° or bank angles near 90°, but are shown to be small for the range of conditions experienced in the approach maneuver. It is also possible that the gimbals be arranged as is shown in figure 5(b), in which the spin axis is again vertical but the pitch angle is measured on the outer gimbal. This arrangement would measure $\int q\, dt$ instead of Euler pitch angle. This measure would also be subject

to deviation depending on the angle of bank and pitch, and it is felt that these deviations would be similar to those incurred by the first arrangement.

Similarly, the Euler yaw angle can be measured by using the gimbal arrangement shown in figure 5(c), in which the spin axis is in the horizontal plane and the yaw angle is measured on the inner gimbal. To use this arrangement a special caging procedure would be required so as to have the spin axis alined in a known direction, preferably in the direction of the runway. Such a procedure would be necessary to avoid locking the inner gimbal, which would occur if the airplane happened to be headed in a direction 90° to the spin axis. It would also be possible to use the arrangement shown in figure 5(d), which approximately measures $\int r\,dt$.

The deviations peculiar to the individual gimbal arrangements were not represented in the equations, but the effects of substituting $\int q\,dt$ for θ_{eu} and $\int r\,dt$ for ψ_{eu} were investigated. For most of the investigation, θ_{eu} and ψ_{eu} were used in the error signals. One inconsistency occurred, in that $\int q\,dt$ was used for the pitch angle in the pitch-angle regulation loop of the autopilot. However, it is felt that this inconsistency would have only a small effect on the results. It should also be noted again that the bank angle used in the bank-angle regulation loop was $\int p\,dt$ and not ϕ_{eu}.

Conditions Investigated

Several different sets of initial conditions were used in the investigation. The first set, which was assumed to represent a normal condition, consisted of a 10-mile range, a 3,000-foot lateral displacement from the center line, and an altitude of 2,900 feet, which is 600 feet above the glide slope. The airplane was assumed to be alined with the runway and flying level. The second case, which was assumed to be a condition that imposed a severe control situation, consisted of a 5-mile range, a 3,000-foot lateral displacement, and an altitude of 1,450 feet, which was 300 feet above the glide slope, and with θ_{eu} and ψ_{eu} again

zero. Lateral displacements to both the left and right of the center line were tried. In all these cases the airplane was assumed to be initially trimmed for level, constant-speed flight.

Several disturbances such as might ordinarily be encountered were also investigated. These included flap deflection, an increase in the slope of the longitudinal force curve C_{X_α}, such as might result from a change in trim angle of attack, random gust disturbances, steady cross winds, noise, and bias errors on the radar signals. In some of these cases the airplane was assumed to be initially flying on the glide-slope center line.

RESULTS

General

The results obtained with the control equations that were selected as being optimum are shown in figures 6 and 7. These results are presented first because of the convenience thereby created for presenting and enlarging on the various features of these control equations. These control equations are

$$\delta_a = -12e_{lat} + 2\psi_{eu} + 2\int p\,dt \quad (e_{lat} < 0.0436) \tag{3a}$$

where

$$e_{lat} = \theta_a + \psi_{eu}$$

$$\delta_a = \mp 0.524 + 2\psi_{eu} + 2\int p\,dt \quad (e_{lat} > 0.0436) \tag{3b}$$

$$\delta_e = -10e_{long} + 2.5(\theta_{eu} + 2.5) + 0.32q + 0.64\int q\,dt \tag{4}$$

where

$$e_{long} = \theta_e + \theta_{eu} + 2.5^\circ$$

$$\delta_r = 0.5r \tag{5}$$

$$\Delta T = (14{,}800 \sin\theta_{eu} - 68\,\Delta V)\frac{1}{1+s} \tag{6}$$

Throughout the figures, where some other control equation is not stated, it should be assumed that the above equations apply.

In figure 6 the initial conditions involve a range of 10 miles, a lateral displacement of 3,000 feet, and a vertical displacement 600 feet above the glide slope. It can be seen that the airplane response and flight-path variations are smooth and well damped, and that the final lateral and longitudinal errors are very small. The airplane initially changes heading about 15° and pitches down about 5°. The pitch angle gradually approaches the desired glide slope of -2.5°, and the radar elevation angle approaches 0°. The 15° heading angle is maintained until the lateral error becomes less than the limit value. At this time the airplane banks so as to decrease the heading angle, and the airplane approaches the center line in a smooth manner. The least desirable feature of the time history is the fairly high initial pitching velocity and rolling velocity that occur. This is partly due to the fact that perfect servos were assumed and therefore instantaneous control deflection occurs at the beginning of the run. However, to a large extent these rotational velocities are due to the basic characteristics inherent in this linear control system and are unavoidable with this system. In the present case the simple nonlinearity introduced by putting a limit on the lateral error alleviates the situation somewhat but not entirely.

Figure 7 presents the results for an initial condition that could be considered severe. These conditions include an initial range of only 5 miles, a lateral displacement of 3,000 feet and a vertical displacement of 300 feet above the glide slope. The flight-path response is such that the lateral error signal contains a lightly damped small-amplitude oscillation over the final part of the run. However, this result is not judged to be unsatisfactory. The disturbance that occurs on the longitudinal error signal near the middle of the run is the result of the change in bank angle that occurs at that point. A divergence occurs in the last few seconds of the run when the range approaches zero. This is to be expected when some error exists when the range approaches zero, and in actual practice some provision would have to be made to eliminate this characteristic, either by returning control to the pilot or by providing a switchover to an automatic touchdown control.

Effect of a Change in the Gain of the Damping Term

The various features of the control laws that are required to achieve the results presented above will be discussed now. Consider first the gains on the damping terms ψ_{eu} and θ_{eu}. As was pointed out before, these terms add damping to the mode of motion relating airplane position to the glide-slope center line. However, they are also attitude-regulating signals so far as the airplane motions are concerned, and can cause short-period oscillations to develop in the motion of the airplane.

Figure 8 shows the effect of varying these gains in the response to an open-loop step input in either lateral or longitudinal error. Figure 8(a) shows that with a gain as high as 6 on ψ_{eu} an undesirable oscillation occurs in the lateral mode of motion of the airplane. It is concluded that with the yaw damping assumed for the augmented airplane, the gain on ψ_{eu} would have to be less than 6. Actually, other considerations, which will be discussed in the following paragraph on limiting the lateral error, restrict the gain on ψ_{eu} even further. In figure 8(b) it is shown that with a gain of 2 on θ_{eu} an oscillation is beginning to develop in the longitudinal mode of motion. A computer limitation made it impractical to try higher gains on this term, but it was concluded that a gain of approximately 2 was as high as could be used on the θ_{eu} term.

Error Signal Gain

The reason for using a limit on the lateral error will now be discussed. Shown in figures 9(a) and 9(b) are the effects of increasing the gain on the lateral error from -6 to -8 with no limit on this term. With a gain of -6, large initial peaks occur in p, q, and α. The peak in q is the result of the peak in e_{long}, which in turn is due to the p term in θ_e as shown in equation (1). The peak in e_{lat} is apparently due to the adverse yaw inherent in the airplane. At a gain of -8 the high response in p and q plus the fact that the problem is nonlinear causes a divergence or extreme oscillation to occur. This time history cannot be considered to be exactly correct because some element of the computer saturated at various times during the run. However, the response was judged to be unsatisfactory. It was felt that the main cause of the oscillation was the coupling between the lateral and longitudinal error signals brought about by the p term in the equation for θ_e. The method used in this investigation to avoid the difficulty was to place a limit on the lateral error. This scheme would limit the rolling velocity, pitching velocity, and bank angle commanded by a large initial error, while at the same time would allow the error gain to be made as large as possible. The large error gain would then insure precise control when the error was reduced to within the limits. Additional roll damping would help also of course, but inasmuch as this approach was not entirely successful, it will be discussed later. The lateral error was therefore arbitrarily limited to a value that would call for no more than 30° of aileron deflection, or a maximum bank angle of 15°. As a consequence of this limit, the maximum yaw-angle change that can be commanded is also limited to a value equal to 30° divided by the gain on the ψ_{eu} term. This maximum change would occur when the

bank angle was 0, of course. In order that the lateral error be corrected as quickly as possible, the gain on ψ_{eu} must be as low as possible so as to allow as large a change in yaw angle as possible. A compromise between the requirements for lateral motion damping and rapid error correction is required. It was found in a typical case that with a gain of -12 on the lateral error and a gain of 1.5 on ψ_{eu}, a divergence occurred when the lateral error came off its stop. A gain of 1.75 on ψ_{eu} gave a response that had satisfactory damping. A gain of 1.75 or 2 with a gain of -12 on the lateral error was therefore used. The use of this limit on the lateral error places a limit on the size of the initial error that can be accommodated by the system. The test case with an initial range of 5 miles and a lateral displacement of 3,000 feet is close to the limit that can be accommodated.

In the longitudinal control law, if a gain of 2.5 is used on the θ_{eu} term, a gain as high as -10 can be used on the longitudinal error and still achieve a deadbeat variation in e_{long}. The constant of 2.5° is added to the θ_{eu} term so as to eliminate the bias error that would result in the glide slope without this constant.

Effect of Changes in the Attitude Quantities

Figure 6 illustrates the effect of using $\int q\,dt$ in the place of θ_{eu} and $\int r\,dt$ in the place of ψ_{eu}. Comparing figures 10(a) and 10(b) shows that the use of $\int q\,dt$ is detrimental to the response, causing a divergence as is shown by the time history of q. A qualitative explanation for this divergence is as follows. Consider first the variation to the error signal, $e_{long} = -10\theta_e - 10\theta_{eu}$, which would occur if the airplane were located stationary on the glide-slope center line and underwent a pitching motion only. The radar elevation angle θ_e is stabilizing and would command a change in elevator deflection which would cause the airplane to return to zero elevation angle. The Euler pitch angle command will cancel the radar-angle command. This arrangement satisfies the condition that, ideally, an airplane rotation alone will not change the error signal. The Euler angle by itself can therefore be thought of as being destabilizing. If the coefficient of the Euler angle were larger than the coefficient of the elevation angle, a divergence would occur. Consider now the circumstances that can cause the

Euler angle term to be larger than the elevation-angle term even though their coefficients are equal. A pitching motion will cause variations in elevation angle and Euler pitch angle according to the following relations:

$$\left.\begin{aligned} \theta_e &= \int -q \cos \theta_a \, dt \\ \theta_{eu} &= \int q \cos \phi_{eu} \, dt \end{aligned}\right\} \tag{7}$$

It can be seen that if an initial radar deflection error θ_a exists, a pitching motion alone will cause a larger variation to occur in θ_{eu} than in θ_e. However, a deflection error will also cause a change in bank angle to occur so that in all practical cases the variation in θ_e will be larger than the variation in θ_{eu} that results from the total motion. However, if $\int q \, dt$ were used instead of θ_{eu} in the error equation, the variation in θ_e would be less than $\int q \, dt$ even though some change in bank angle did occur. The error signal would therefore be destabilizing, and a divergence could occur.

The use of $\int r \, dt$ (fig. 6(c)) in the place of ψ_{eu} has little apparent effect on the resulting motions. An analysis of the lateral error signal similar to that given above for the longitudinal error signal would show that the variation in θ_a due to a yaw motion would always be larger than the variation in either ψ_{eu} or $\int r \, dt$. As was stated before, θ_{eu} and ψ_{eu} were used throughout the investigation.

Airspeed Control

Since the six-degree-of-freedom representation for the airplane allowed changes in airspeed to occur, it was necessary that some provision be made to regulate the airspeed. A comparison of figures 11(a) and 11(b) shows the effect of not having any provision for airspeed

regulation. With no airspeed control the velocity diverges and consequently the longitudinal error is not reduced. The primary provision for airspeed regulation was the variation of thrust as a function of Euler pitch angle so that the longitudinal component of gravity would be canceled. To this throttle control is added an airspeed feedback term to take care of changes in drag due to change in angle of attack. Figure 11(c) shows that, with this gain, this velocity feedback by itself can regulate the velocity during a typical maneuver fairly well, but not well enough for a successful approach to be made. Figure 11(d) shows that the θ_{eu} command by itself causes fairly large thrust changes and regulates the velocity closer than the airspeed feedback by itself does. The combination of the two signals keeps the velocity change within 3 feet per second during a typical run. The change in thrust shown in figure 11(a) corresponds to a change in revolutions per minute from 83 percent to 70 percent for a typical engine. It could be concluded that the velocity feedback was not necessary for successful completion of the typical case shown in figure 11. However, in other circumstances which will be discussed later, the velocity feedback was more necessary. Also, in these example cases, the gain on the θ_{eu} term in the throttle control was made to match exactly the assumed weight of the airplane. In actual practice this situation would not always be present, and this is another reason for having an airspeed feedback, to adjust for the different throttle settings that would be required by the effect of varying airplane weight.

Disturbances

In addition to the general control disturbances that result from the various initial conditions described in the previous paragraphs, several miscellaneous disturbances to which an airplane can be subjected were also examined. The first of these is the deflection of the landing flaps. In the previous cases the airplane was assumed to be trimmed initially with the flaps deflected. In the present case it is assumed that the airplane is trimmed at the same airspeed with flaps up, and at zero time the flaps are deflected instantaneously. This action is represented in the equations of motion by adding suitable constants to the lift, drag, and pitching-moment equations. Also, in this case the airplane was assumed to be initially flying along the glide-slope center line. As is shown in figure 12, after the flap is deflected the airplane trims at a new angle of attack and airspeed. The airplane also rises above the glide slope and approaches the ground with a glide slope 0.01 radian higher than normal. No particular difficulty is encountered in this case.

In the next case the slope of the longitudinal force curve C_{X_α} is changed from a positive value to an equal negative value. This change represents the change in slope that would occur with some increase in trim angle of attack and represents a condition where the drag force $\frac{1}{2}\rho V^2 C_D$ for 1 g flight increases with a decrease in airspeed. As is

shown in figure 13(a), the response of the airplane is satisfactory. Comparing figure 13(a) with figure 7 shows that some changes occurred in the angle of attack and velocity time history, but these changes were minor. In this case the airspeed feedback in the throttle control was necessary, as is illustrated by figure 13(b), which shows that without this airspeed feedback the response was unsatisfactory. Without the airspeed feedback the velocity and angle of attack, and consequently, the longitudinal error, diverged.

Another type of disturbance which has a large effect on the precise control of an airplane is the gust disturbance. Therefore, the effect of both random gust disturbances and steady cross winds was studied. Random disturbances were added to the β and α inputs to the airplane equations so as to simulate side gusts and vertical gusts. However, no attempt was made to represent the effect of lag due to penetration nor lag in gust effect on the tail of the airplane. The random inputs were generated by a noise generator which had a flat power spectrum out to 30 cycles per second. The amplitude of the output of the noise generator was shaped with a first-order filter so that a break occurred in the power spectrum at a frequency that corresponded to a gust wave length of 6,000 feet. The gust inputs therefore approximately correspond to the measured gust characteristics reported in reference 2.

Five different time histories which show the effect of random side gust inputs with root-mean-square values of 3 and 6 feet per second are presented in figure 14. Note that total sideslip is equal to the sum of the sideslip which would be experienced in still air and sideslip due to gusts in these cases, that is,

$$\beta_t = \bar{\beta} + \beta_g \tag{8}$$

and that it is $\bar{\beta}$ that is plotted in these figures. The gust noise excites the short-period lateral and longitudinal modes of motions, but has little or no effect on the mode of motion relating airplane position to the glide-slope center line. The measured mean square of the disturbance is also plotted in figure 10(a).

The effect of random vertical gusts with root-mean-square values of 6 feet per second is shown in figure 15. Some disturbance to the vertical position of the airplane can be noted near the end of the runs in these cases. For example, in the second run the longitudinal error reaches a value of 0.01 radian for an instant at short range. However, no serious effects were encountered.

The effect of lateral cross winds of 20 and 30 feet per second is shown in figure 16. These cross winds cause the airplane to be pushed off the center line. The result is that the airplane approaches the

runway at angles of approximately 0.015 and 0.025 radian, respectively, from the center line. No other difficulties were noted.

The effect of vertical winds of 10 and -20 feet per second is shown in figure 17. Downward winds of 20 feet per second caused relatively large vertical position errors to occur at short range, and an instability occurred. Note that the oscillation appears to start in the lateral error, and therefore apparently depends on some random lateral disturbance, which in this case is probably computer noise. Further evidence of this dependency is offered by that fact that the time history could not be consistently repeated. Of course, in actual practice lateral disturbances would always be present.

The extreme conditions that are necessary to make this instability appear in the calculated time histories are not likely to be encountered in actual practice. However, the demonstrated tendency for this instability to occur indicates that a remedy might be necessary. The remedy that was tried consisted of putting a first-order filter on the θ_{eu} term in the elevator command equation. This term is needed to damp the long period motion which describes the position of the airplane with respect to the glide slope, but it is also an attitude signal with respect to the short-period motion of the airplane itself. It was felt that since the filter would allow the low-frequency variation in θ_{eu} to pass while it attenuated the high-frequency variation, the necessary damping would be retained while the tendency for short-period oscillation to develop would be reduced. Figure 18(a) shows that a filter with a time constant of 2 seconds did eliminate the instability even when a vertical wind of -30 feet per second was assumed. When a 3-second time constant was used, the result was an unstable oscillation, similar in appearance to the oscillation experienced with no lag term. It was concluded that the 3-second time constant cut off too much of the low frequency θ_{eu} signal. Even though the filter with the 2-second time constant improved the response of the airplane in the presence of gusts, it deteriorated the response to an initial displacement, as is shown in figure 18(b).

The addition of noise with a root-mean-square value of 0.045 radian to the radar angle signals had little or no effect. Therefore, no figures are given. It was felt that it was beyond the scope of the present investigation to study any other radar deficiencies that might affect the system.

Additional Roll Damping

As was stated earlier, fairly large initial peaks occurred in time histories in which an initial displacement from the glide-slope center line was present. Adding roll damping to the airplane should decrease

the amplitude of these peaks. Figure 19 shows that such an addition does indeed reduce them. However, the additional roll damping reduces the speed of the lateral response and thereby also reduces the precision with which the lateral position of the airplane is controlled as is shown in figure 20 in which a random lateral gust input is included. A small but apparent bias error is evident in the last half of these time histories which was not present when no additional roll damping was used. The addition of roll damping apparently is also incompatible with the use of the first-order filter on the θ_{eu} term to eliminate the instability that was caused by the vertical wind. Figure 21 shows that this combination resulted in an instability which did not occur when no additional roll damping was used.

CONCLUDING REMARKS

An analysis of an automatic approach system, which uses information of the type that can be obtained by using airborne radar tracking a target at the end of the runway and attitude-measuring gyros carried in the airplane, shows that such a control system is feasible. An idea of the maximum permissible gains for the control terms relating control surface deflection to displacement from the glide-slope center line can be obtained from the example used in the paper. These particular gains are related to the control effectiveness and the dynamics of the airplane-autopilot combination used in the example. Any variation in these factors would require some change in the gains. It was necessary to put a limit on the value of the lateral error used in the control equation to achieve satisfactory results. This limit places a restriction on the area from which a successful approach can be initiated but in exchange for the restriction, allows more precise control. It was also shown that the attitude measurements necessary for determining the error signals must be measurements of Euler angles rather than the integral of body axes rotations for successful completion of the task. An instability was indicated under the circumstances of extremely large longitudinal error at short range. To correct for this condition a first-order filter was placed on the damping term θ_{eu}. This term is, of course, an attitude signal so far as the modes of motion of the airplane alone are concerned, and therefore can induce a tendency for short-period oscillations to develop. By putting a first-order filter on θ_{eu} this tendency is reduced. Disturbances such as random gusts, steady cross winds, flap deflection, and radar noise were also investigated, and except for the instability mentioned before, no difficulties nor unsatisfactory conditions were encountered.

This analysis has been made as realistic as possible by considering most of the nonlinearities introduced by radar and gyro gimbal effects, the complete equations of motion of the airplane, and the effects of gust

disturbances and initial alinement errors. The results show that unexpected instabilities occur involving nonlinear oscillations and that the careful adjustment of system parameters is necessary to obtain successful results. In the development of an actual system which utilizes the principles considered in this paper, and in which maximum performance in the way of precision and rapid response is desired, an analog-computer investigation such as reported herein appears indispensable as a means of predicting and avoiding difficulties.

Langley Research Center,
National Aeronautics and Space Administration,
Langley Field, Va., July 16, 1959.

APPENDIX A

SYMBOLS

m	mass, slugs
S	wing area, sq ft
$\bar{c}$	mean aerodynamic chord, ft
b	wing span, ft
V	velocity, ft/sec
I_X, I_Y, I_Z	moments of inertia, slug-ft^2
K_X, K_Y, K_Z	nondimensional radius of gyration
F_X	axial force, lb
F_Y	side force, lb
F_Z	normal force, lb
M_X	rolling moment, ft-lb
M_Y	pitching moment, ft-lb
M_Z	yawing moment, ft-lb

$$C_X = \frac{F_X}{\frac{1}{2}\rho S V_o^2}$$

$$C_Z = \frac{F_Z}{\frac{1}{2}\rho S V_o^2}$$

$$C_Y = \frac{F_Y}{\frac{1}{2}\rho S V_o^2}$$

$$C_l = \frac{M_X}{\frac{1}{2}\rho S V_o^2 b}$$

$$C_m = \frac{M_Y}{\frac{1}{2}\rho S V_o^2 \bar{c}}$$

$$C_n = \frac{M_Z}{\frac{1}{2}\rho S b V_o^2}$$

ρ	air density, slugs/cu ft
T	thrust, lb
t	time, sec
p	rolling velocity, radians/sec
q	pitching velocity, radians/sec
r	yawing velocity, radians/sec
α	angle of attack, radians
β	angle of sideslip, radians
$\bar{\alpha}$	angle between X-axis and velocity vector V; that is, angle of attack in still air
$\bar{\beta}$	angle between X-axis and velocity vector V; that is, angle of sideslip in still air
$\psi_{eu}, \theta_{eu}, \phi_{eu}$	Euler angles, radians (fig. 4)
θ_e	radar elevation angle, radians (fig. 3)
θ_a	radar deflection angle, radians
u,v,w	perturbation velocity components along the X, Y, and Z axes, ft/sec
R	range, miles

δ_a	total aileron deflection, radians
δ_e	elevator deflection, radians
δ_r	rudder deflection, radians
s	Laplace operator, per sec
D	nondimensional operator
e_{long}	longitudinal steering error, radians
e_{lat}	lateral steering error, radians
ms	mean-square value of disturbance
rms	root-mean-square value of disturbance
Ω	rotation of the line of sight
ζ	damping ratio
P	period, sec
$K_1, K_2, \ldots K_{11}$	constants
X,Y,Z	body axes
X_r, Y_r, Z_r	radar axes
X_e, Y_e, Z_e	earth axes

Subscripts:

o	initial condition
g	gust
t	total

Dot over quantity indicates differentiation with respect to time.

Stability derivatives are indicated by subscript notation; for example:

$$C_{Z_\alpha} = \frac{\partial C_Z}{\partial \alpha}$$

$$C_{n_r} = \frac{\partial C_n}{\partial \frac{rb}{2V}}$$

APPENDIX B

EQUATIONS

The equations used in the investigation are presented below. The airplane equations are written about body axes, which are assumed to be the principal axes also. All stability derivatives were obtained from data or calculated for the airplane in the landing configuration at an angle of attack of 9°. The small initial gravity vectors, Euler angles, and radar angles that would be caused by an initial angle of attack are neglected. In this respect the equations may be thought of as being written for an airplane with enough wing incidence so that the wing can support the airplane at the assumed airspeed with the body axes alined with the wind and earth axes. Inertia coupling terms and the wq term in the X-axis equation were left out because it was felt that they were negligible, and their omission simplified the solution of the equations.

Airplane six-degree-of-freedom equations are given below:

$$\frac{m}{\frac{1}{2}\rho S\bar{c}}\frac{\bar{c}}{V_o}\frac{\dot{u}}{V_o} = C_{X_{(u/V_o)}}\frac{u}{V_o} + C_{X_\alpha}\alpha + C_{Z,o}\sin\theta_{eu} + \frac{\Delta T}{\frac{1}{2}\rho V^2 S}$$

$$\frac{m}{\frac{1}{2}\rho S\bar{c}}\frac{\bar{c}}{V_o}\left(\dot{\alpha} - q\right) = C_{Z_{(u/V_o)}}\frac{u}{V_o} + C_{Z_\alpha}\alpha - C_{Z,o}\cos\theta_{eu}\cos\phi_{eu} + C_{Z_{\delta_e}}\delta_e + C_{Z,o}$$

$$\frac{m}{\frac{1}{2}\rho S\bar{c}}\left(\frac{\bar{c}}{V_o}\right)^2 K_Y{}^2\dot{q} = C_{m_{(u/V_o)}}\frac{u}{V_o} + C_{m_\alpha}\alpha + \frac{\bar{c}}{2V_o}C_{m_{D\alpha}}\dot{\alpha} + \frac{\bar{c}}{2V_o}C_{m_q}q + C_{m_{\delta_e}}\delta_e$$

$$\frac{m}{\frac{1}{2}\rho Sb}\frac{b}{V_o}\left(\dot{\beta} + r\right) = C_{Y_\beta}\beta - C_{Z,o}\cos\theta_{eu}\sin\phi_{eu} + C_{Y_{\delta_r}}\delta_r$$

$$\frac{m}{\frac{1}{2}\rho Sb}\left(\frac{b}{V_o}\right)^2 K_Z{}^2\dot{r} = C_{n_\beta}\beta + \frac{b}{2V_o}C_{n_r}r + \frac{b}{2V_o}C_{n_p}p + C_{n_{\delta_r}}\delta_r$$

$$\frac{m}{\frac{1}{2}\rho Sb}\left(\frac{b}{V_o}\right)^2 K_X{}^2\dot{p} = C_{l_\beta}\beta + \frac{b}{2V_o}C_{l_r}r + \frac{b}{2V_o}C_{l_p}p + C_{l_{\delta_r}}\delta_r + C_{l_{\delta_a}}\delta_a$$

where

$m = \frac{14{,}800}{32.2}$ slugs

$C_{Z_o} = -0.91$

$\bar{c} = 8.96$ ft

$V_o = 212$ ft/sec

$K_Y^2 = 0.722$

$K_Z^2 = 0.062$

$K_X^2 = 0.0167$

$\frac{\partial T}{\partial V} = -3.3$ lb/ft/sec

$C_{X_{(u/V_o)}} = \frac{T_V V_o}{\frac{1}{2}\rho S V_o^2} + 2C_{X,o} = -0.154$

$C_{X_\alpha} = 0.63$

$C_{Z_{(u/V_o)}} = 2C_{Z,o} = -1.82$

$C_{Z_\alpha} = -3.62$

$C_{Z_{\delta_e}} = -0.172$

$C_{m_{(u/V_o)}} = 0$

$C_{m_\alpha} = -0.287$

$C_{m_{D\alpha}} = -2.0$

$S = 300$ sq ft

$b = 34.5$ ft

$I_Y = 26{,}676$ slug-ft^2

$I_Z = 33{,}943$ slug-ft^2

$I_X = 9{,}148$ slug-ft^2

$C_{X,o} = -0.055$

$C_{Y_\beta} = -0.92$

$C_{Y_{\delta_r}} = 0.247$

$C_{n_\beta} = 0.086$

$C_{n_r} = -0.24$

$C_{n_p} = -0.15$

$C_{n_{\delta_r}} = -0.10$

$C_{l_\beta} = -0.086$

$C_{l_r} = 0.15$

$C_{l_p} = -0.375$

$C_{l_{\delta_r}} = 0.011$

$C_{m_q} = -4.0$ $\qquad$ $C_{l_{\delta_a}} = -0.046$

$C_{m_{\delta_e}} = -0.373$

The airplane equations with numerical coefficients inserted become

$$6.05s \frac{u}{V_o} = -0.154 \frac{u}{V_o} + 0.63\alpha - 0.91 \sin \theta_{eu} + 0.000062 \Delta T \qquad (9)$$

$$6.05(s\bar{\alpha} - q) = -1.82 \frac{u}{V_o} - 3.62\alpha + 0.91 \cos \theta_{eu} \cos \phi_{eu} - 0.172\delta_e - 0.91 \qquad (10)$$

$$0.186sq = -0.287\alpha - 0.0423s\alpha - 0.0846q - 0.373\delta_e \qquad (11)$$

$$6.05(s\bar{\beta} + r) = -0.92\beta + 0.91 \cos \theta_{eu} \sin \phi_{eu} + 0.247\delta_r \qquad (12)$$

$$0.061sr = 0.086\beta - 0.0195r - 0.0122p - 0.10\delta_r \qquad (13)$$

$$0.0164sp = -0.086\beta + 0.0122r - 0.0304p + 0.011\delta_r - 0.046\delta_a \qquad (14)$$

The Euler angles are determined from the calculated motions about the body axes in the following manner:

Let

$$l_3 = -\sin \theta_{eu}$$

$$m_3 = \cos \theta_{eu} \sin \phi_{eu}$$

$$n_3 = \cos \theta_{eu} \cos \phi_{eu}$$

Then

$$\dot{l}_3 = m_3 r - n_3 q \qquad (15)$$

$$\dot{m}_3 = n_3 p - l_3 r \qquad (16)$$

$$\dot{n}_3 = l_3 q - m_3 p \qquad (17)$$

$$\dot{\Psi}_{eu} = \frac{rn_3 + qm_3}{1 - l_3^2} \tag{18}$$

$$\dot{\phi}_{eu} = p - l_3\dot{\Psi}_{eu} \tag{19}$$

$$\dot{\theta}_{eu} = \frac{qn_3 - rm_3}{\sqrt{1 - l_3^2}} \tag{20}$$

$$\Psi_{eu} = \Psi_{eu_o} + \int \dot{\Psi}_{eu}\, dt \tag{21}$$

$$\phi_{eu} = \phi_{eu_o} + \int \dot{\phi}_{eu}\, dt \tag{22}$$

$$\theta_{eu} = \theta_{eu_o} + \int \dot{\theta}_{eu}\, dt \tag{23}$$

The above equations are convenient for use on an analog computer. More descriptive equations are as follows:

$$\dot{\Psi}_{eu} = r\,\frac{\cos \phi_{eu}}{\cos \theta_{eu}} + q\,\frac{\sin \phi_{eu}}{\cos \theta_{eu}}$$

$$\dot{\phi}_{eu} = p + q \tan \theta_{eu} \sin \phi_{eu} + r \tan \theta_{eu} \cos \phi_{eu}$$

$$\dot{\theta}_{eu} = q \cos \phi_{eu} - r \sin \phi_{eu}$$

The radar angles are determined as follows:

The velocities along the body axes are

$$V_X = V_o\left(1 + \frac{u}{V_o}\right) \tag{24}$$

$$V_Y = V_o\left(1 + \frac{u}{V_o}\right)\sin \bar{\beta} \tag{25}$$

$$V_Z = V_o\left(1 + \frac{u}{V_o}\right)\sin \bar{\alpha} \tag{26}$$

The velocities along the radar axes are

$$V_{X_r} = V_X \cos \theta_a \cos \theta_e + V_Y \sin \theta_a \cos \theta_e - V_Z \sin \theta_e \tag{27}$$

$$V_{Y_r} = -V_X \sin \theta_a + V_Y \cos \theta_a \tag{28}$$

$$V_{Z_r} = V_X \cos \theta_a \sin \theta_e + V_Y \sin \theta_a \sin \theta_e + V_Z \cos \theta_e \tag{29}$$

Then

$$R = R_o - \int V_{X_r}\, dt \tag{30}$$

$$\Omega_{Z_r} = -\frac{V_{Y_r}}{R} \tag{31}$$

$$\Omega_{Y_r} = \frac{V_{Z_r}}{R} \tag{32}$$

$$\theta_a = \theta_{a,o} + \int \left[\Omega_{Z_r} \sec \theta_e - r - (q \sin \theta_a + p \cos \theta_a)\tan \theta_e\right] dt \tag{33}$$

$$\theta_e = \theta_{e,o} + \int \left(\Omega_{Y_r} - q \cos \theta_a + p \sin \theta_a\right) dt \tag{34}$$

The control equations are

$$e_{long} = \theta_{eu} + \theta_e + 2\tfrac{1}{2}^o \tag{35}$$

$$e_{lat} = \psi_{eu} + \theta_a \tag{36}$$

$$\delta_e = K_1 e_{long} + K_2 \theta_{eu} + K_3 q + K_4 \int q\, dt \tag{37}$$

$$\delta_a = K_5 e_{lat} + K_6 \psi_{eu} + K_7 \int p \, dt + K_8 p \tag{38}$$

$$\delta_r = K_9 r \tag{39}$$

$$\Delta T = \left(K_{10} \sin \theta_{eu} + K_{11} V_o \frac{u}{V_o} \right) \frac{1}{1 + s} \tag{40}$$

When lateral gust inputs are used, the following substitutions are made:

$$\beta_t = \bar{\beta} + \beta_g$$

and β_t is substituted for β in equations (12), (13), and (14).

When vertical gust inputs are used, the following substitutions are made:

$$\alpha_t = \bar{\alpha} + \alpha_g$$

and α_t is substituted for α in equations (9), (10), and (11).

When radar noise or bias errors are used, the following substitutions are made:

$$\theta_e' = \theta_e + \text{Noise}$$

and θ_e' is substituted for θ_e in equations (35) and (37).

$$\theta_a' = \theta_a + \text{Noise}$$

and θ_a' is substituted for θ_a in equations (36) and (38).

REFERENCES

1. Abzug, Malcolm J.: Applications of Matrix Operators to the Kinematics of Airplane Motion. Jour. Aero. Sci., vol. 23, no. 7, July 1956, pp. 679-684.

2. Crane, Harold L., and Chilton, Robert G.: Measurements of Atmospheric Turbulence Over a Wide Range of Wavelength for One Meteorological Condition. NACA TN 3702, 1956.

TABLE I.- AIRPLANE CHARACTERISTICS

Configuration	P, sec	ζ	Other roots
Longitudinal			
Airplane alone	32.2 4.65	0.029 .485	
Airplane + pitch damper + pitch attitude	31 3.6	0.625 .47	
Airplane + pitch damper + pitch attitude + throttle control	46.5 3.6	0.98 .47	
Lateral			
Airplane alone	4.33	0.054	s + 2.15 s + 0.0153
Airplane + yaw damper + roll attitude	4.65 2.73	0.624 .345	
Airplane + yaw damper + roll attitude + roll damper	4.72 2.63	0.575 .782	

Autopilot Gains

δ_e/Pitch angle = 0.064 radian/radian

δ_e/Pitch velocity = 0.32 radian/radian/sec

δ_r/Yawing velocity = 0.5 radian/radian/sec

δ_a/Roll angle = 2 radian/radian

δ_a/Rolling velocity = 0.7 radian/radian/sec

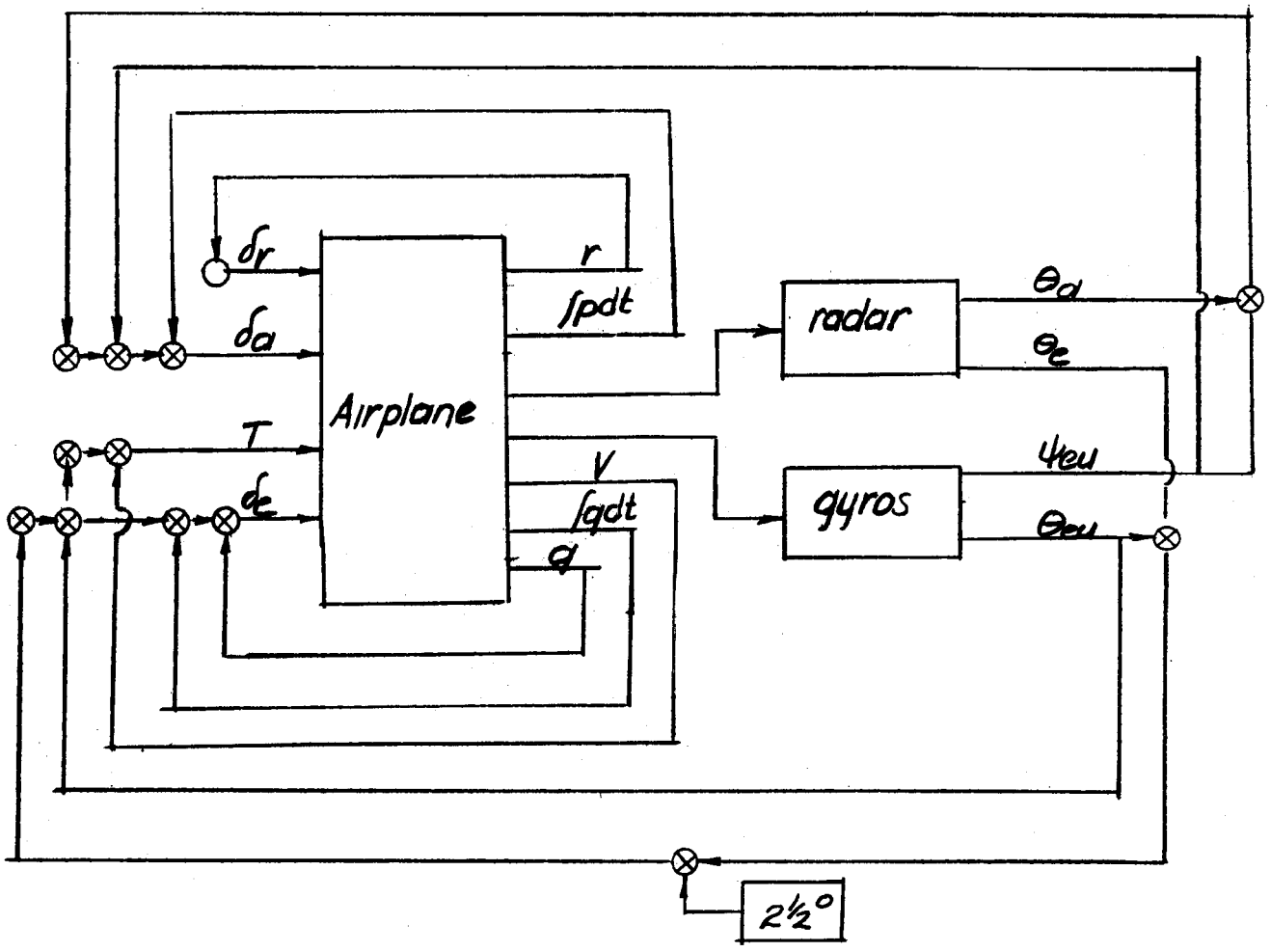

Figure 1.- Block diagram of automatic approach system.

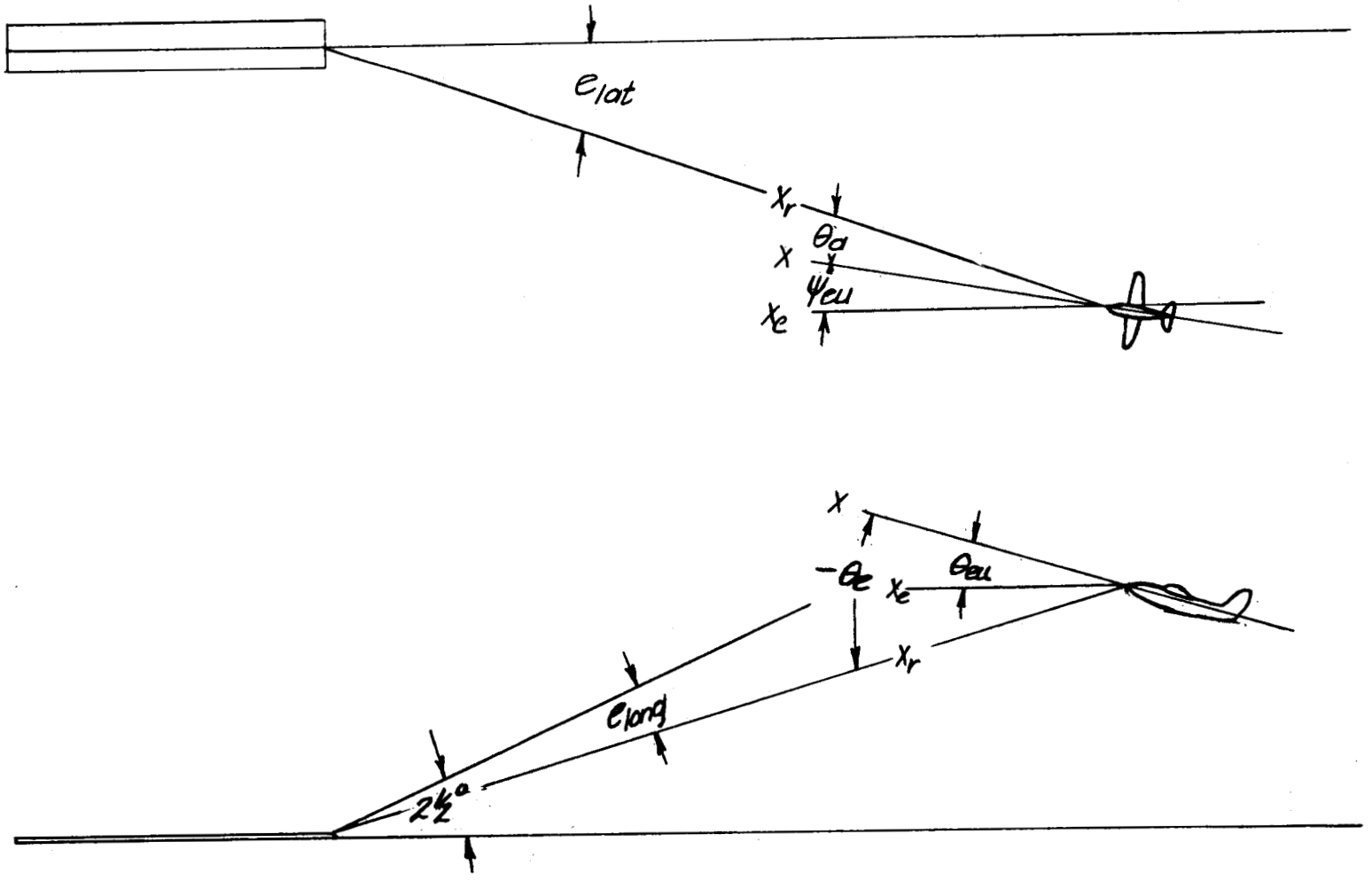

Figure 2.- Geometry of approach problem.

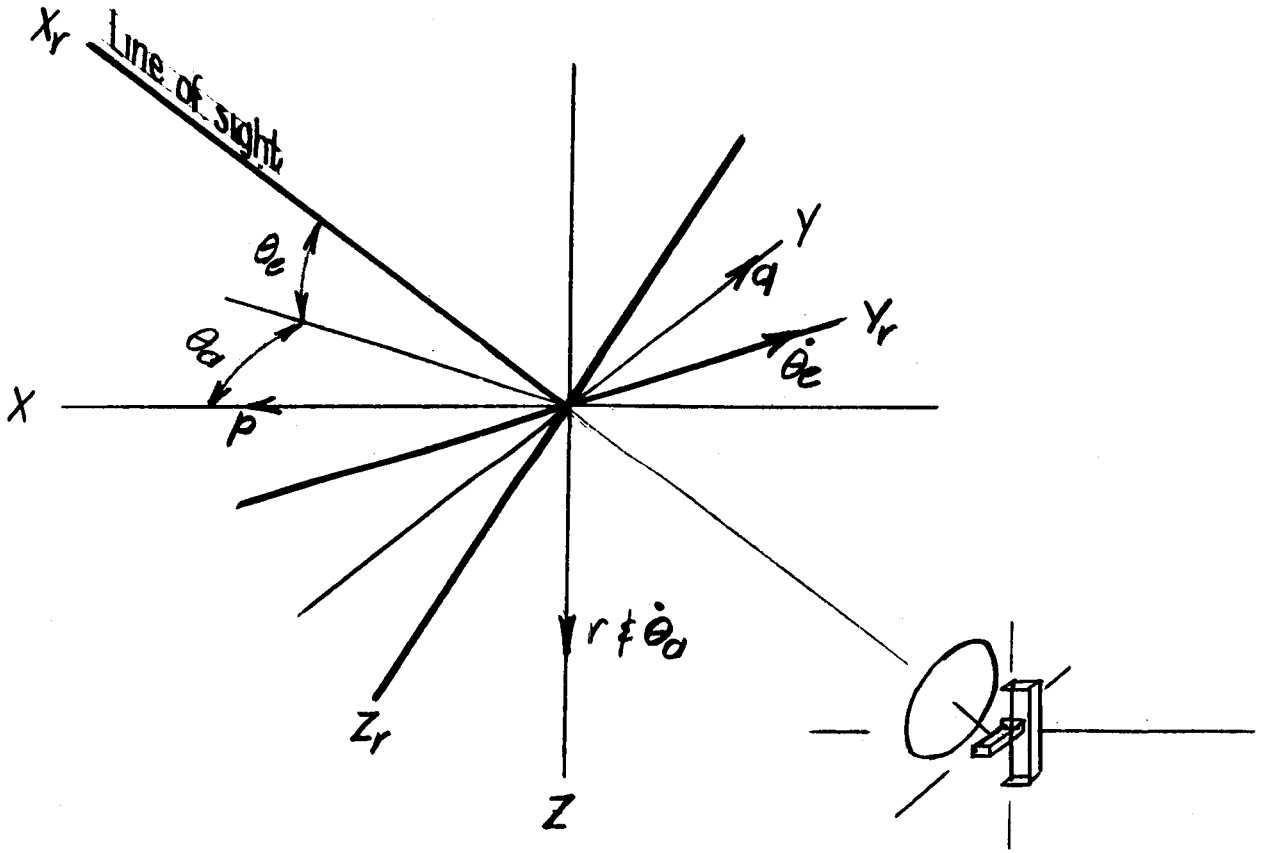

Figure 3.- Definition of radar angles and sketch of gimbal arrangement.

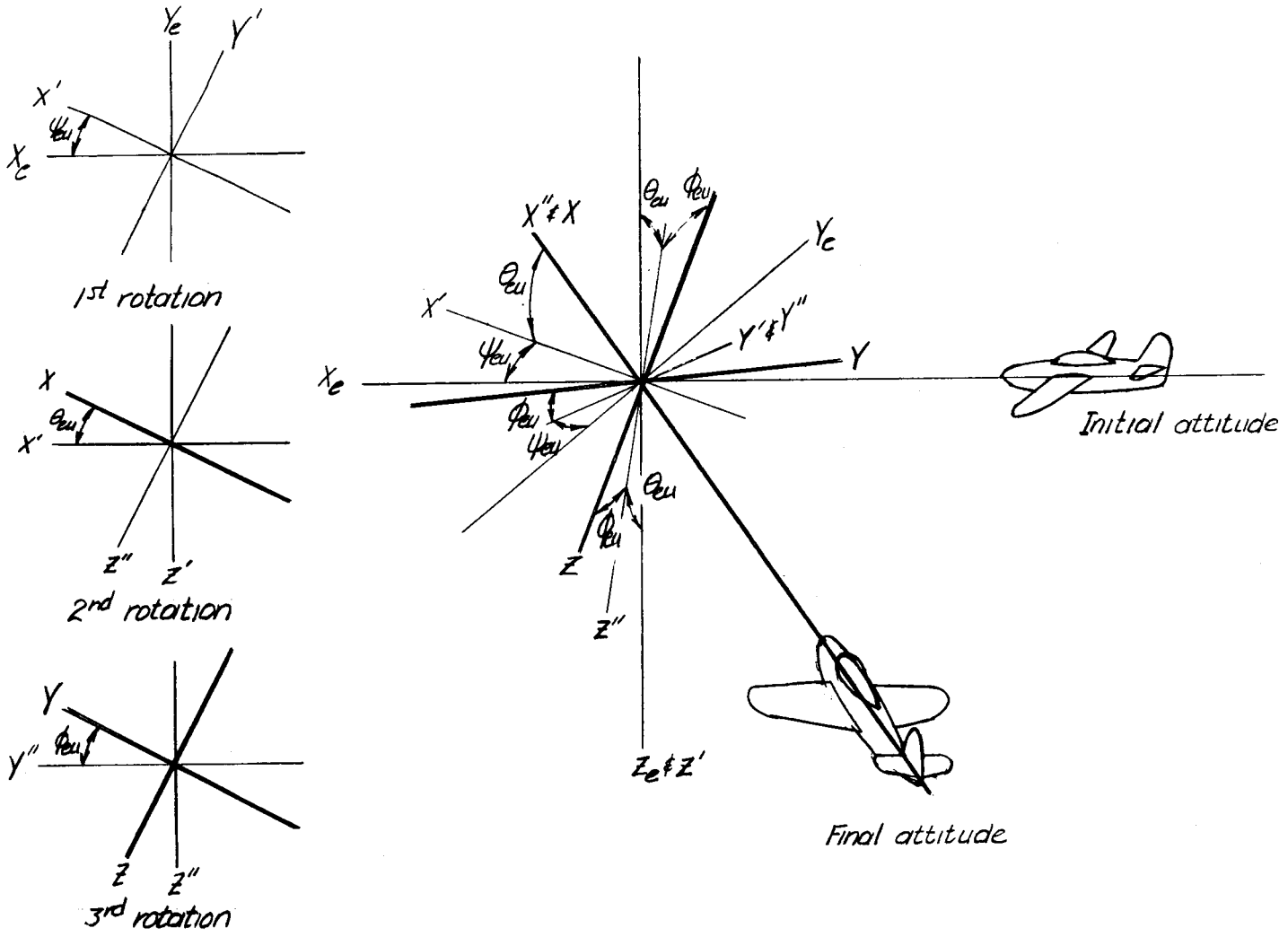

Figure 4.- Definition of Euler angles which define orientation of body axes with respect to initial or earth axes.

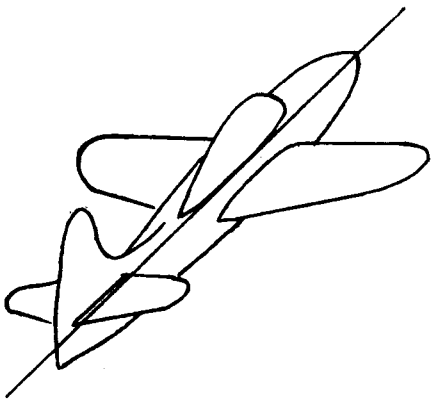

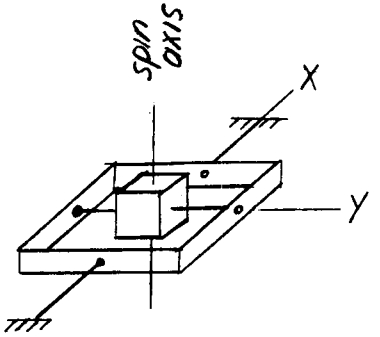

(a) inner gimbal - Θ_{eu}
outer gimbal - $\int p\,dt$

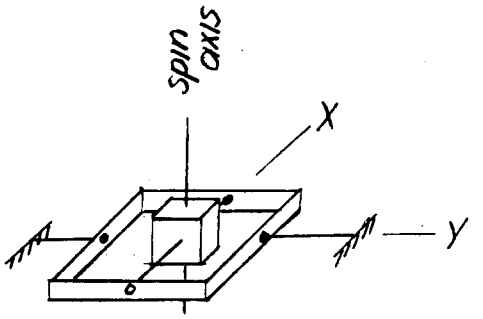

(b) inner gimbal - Φ_{eu}
outer gimbal - $\int q\,dt$

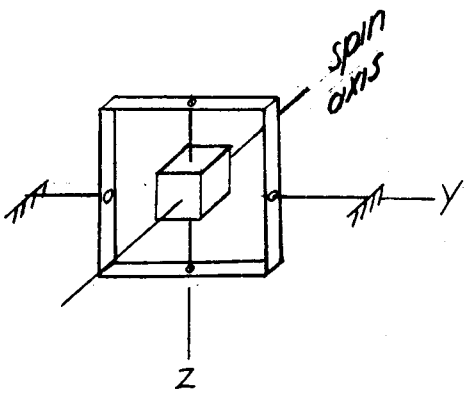

(c) inner gimbal - Ψ_{eu}

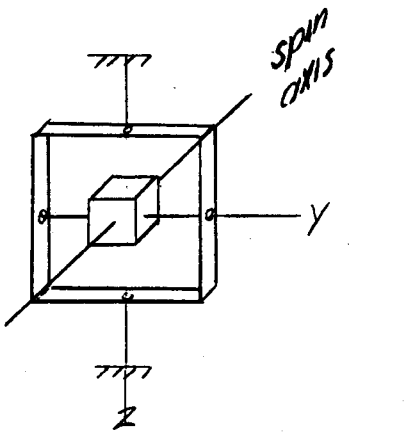

(d) outer gimbal - $\int r\,dt$

Figure 5.- Various gyro gimbal arrangements.

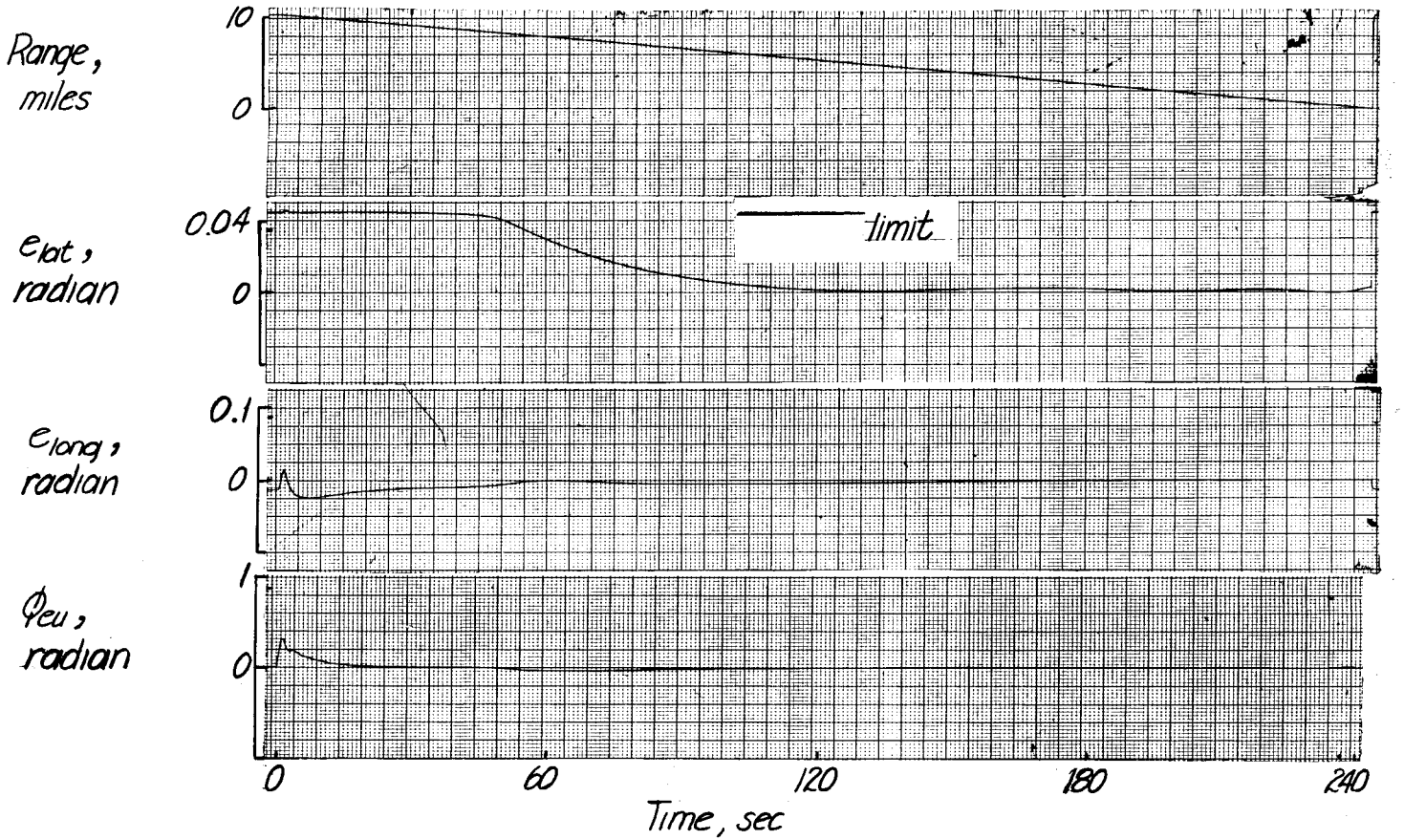

Figure 6.- Typical approach at long range. $\theta_{a,o} = 3.25^{\circ}$; $\theta_{e,o} = -3.14^{\circ}$; $\theta_{eu,o} = \psi_{eu,o} = \phi_{eu,o} = 0^{\circ}$; R = 10 miles; $\delta_a = -12e_{lat} + 2\psi_{eu} + 2\int p\,dt$; $\delta_e = -10e_{long} + 2.5(\theta_{eu} + 2.5^{\circ}) + 0.32q + 0.64\int q\,dt$.

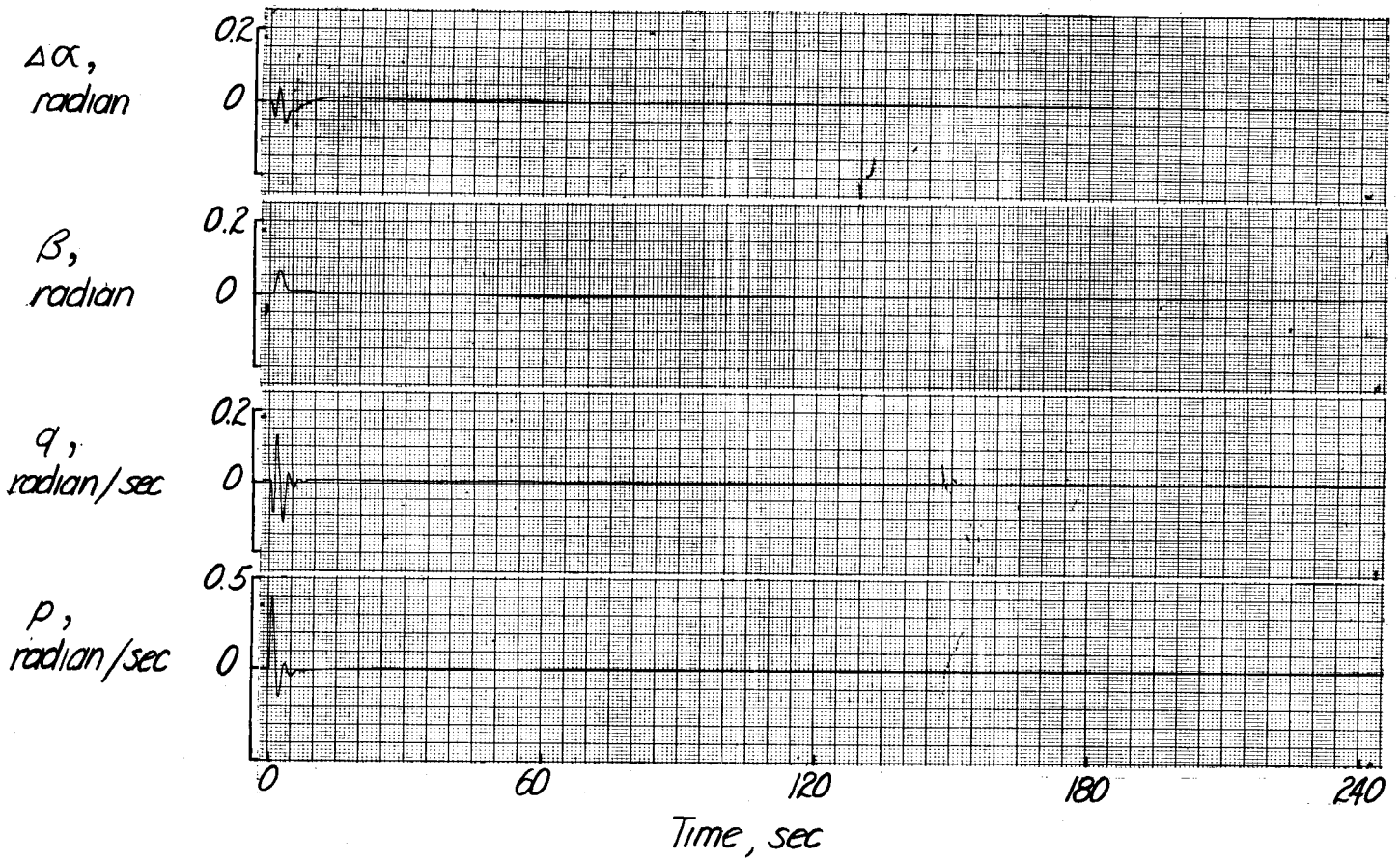

Figure 6.- Continued.

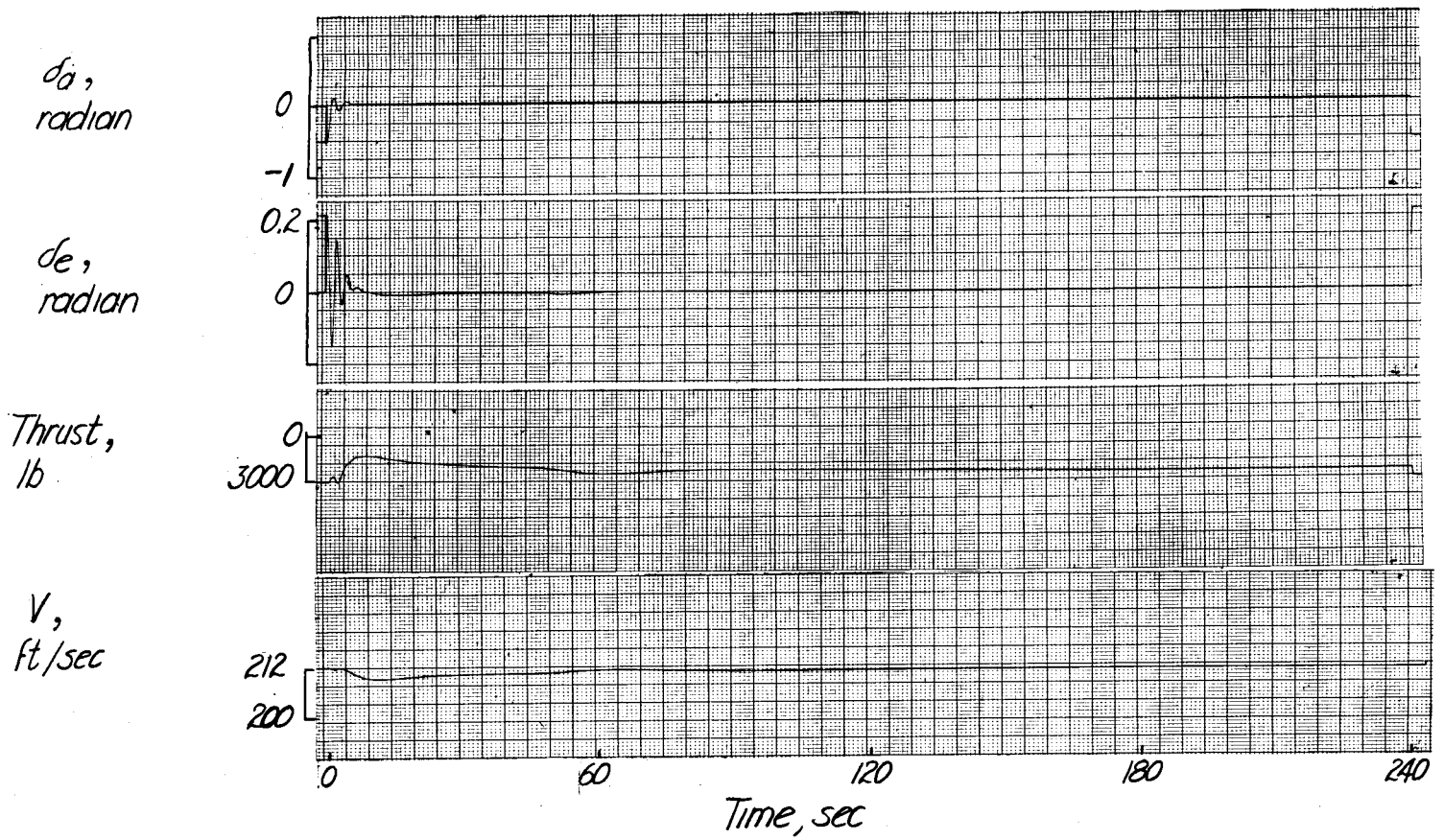

Figure 6.- Continued.

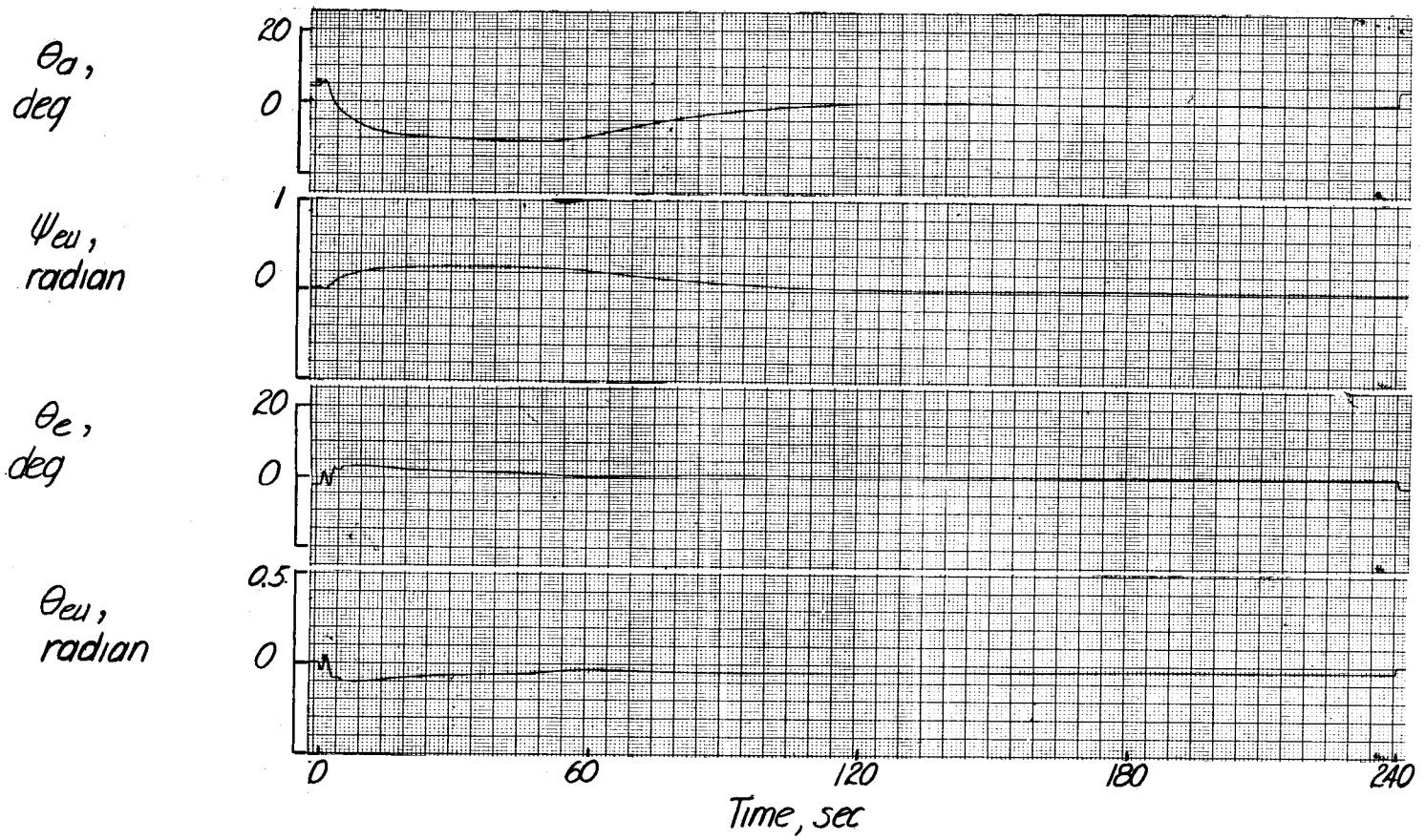

Figure 6.- Concluded.

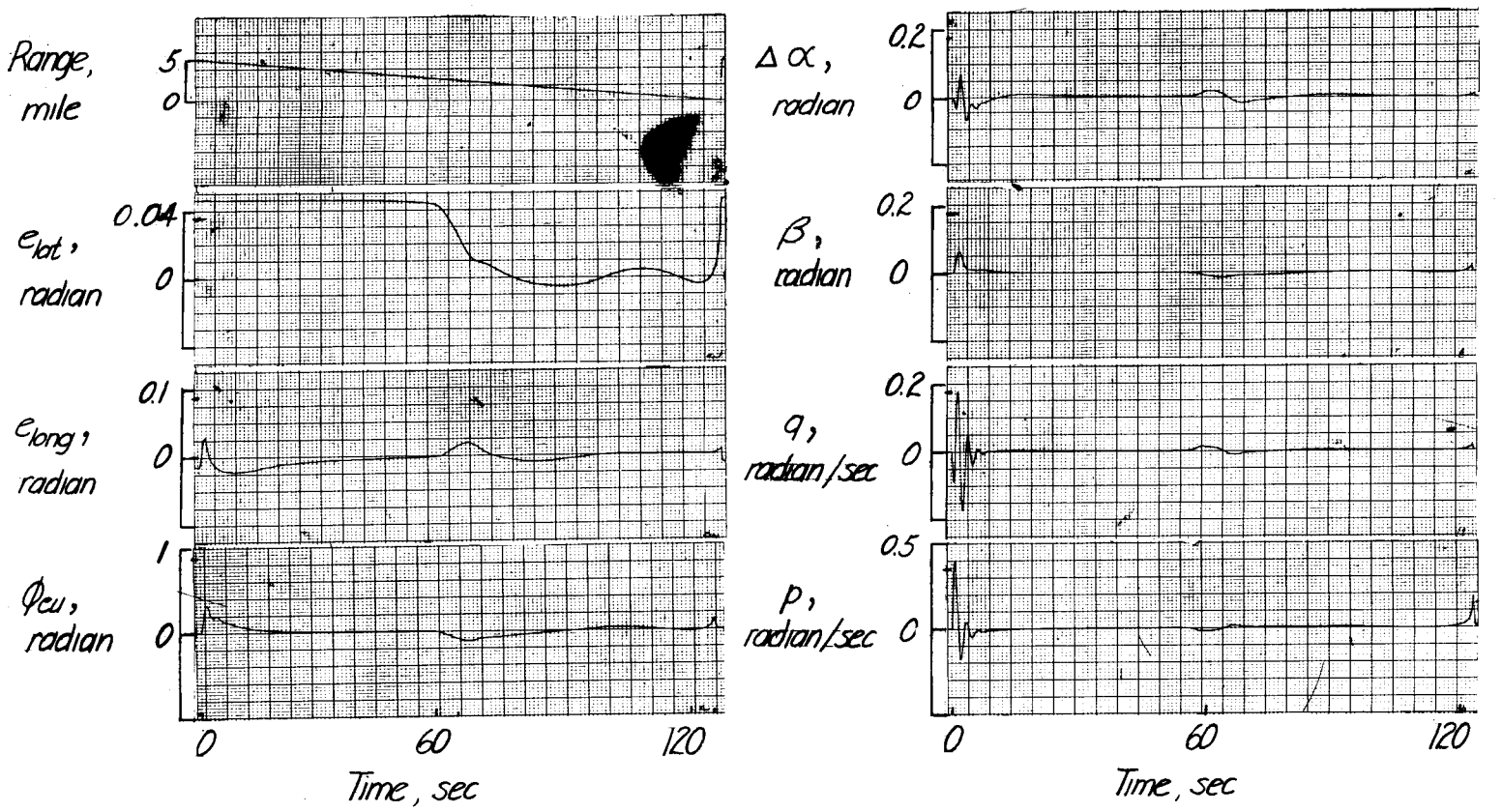

Figure 7.- Typical approach at short range. $\theta_{a,o} = 6.52^{o}$; $\theta_{e,o} = -3.14^{o}$;

$\theta_{eu,o} = \Psi_{eu,o} = \phi_{eu,o} = 0^{o}$; R = 5 miles; $\delta_a = -12e_{lat} + 2\Psi_{eu} + 2\int p\,dt$;

$\delta_e = -10e_{long} + 2.5(\theta_{eu} + 2.5^{o}) + 0.32q + 0.64\int q\,dt$.

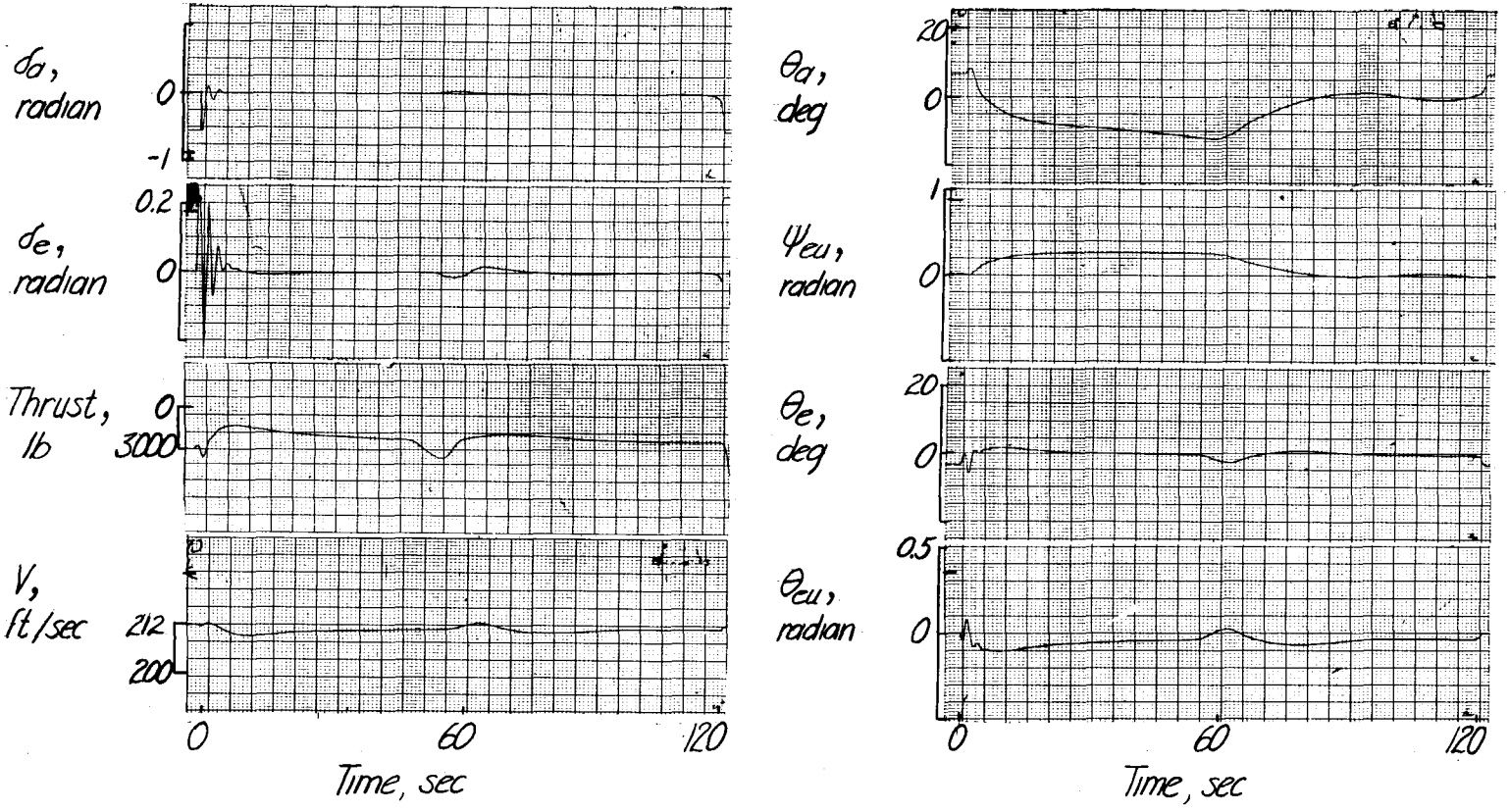

Figure 7.- Concluded.

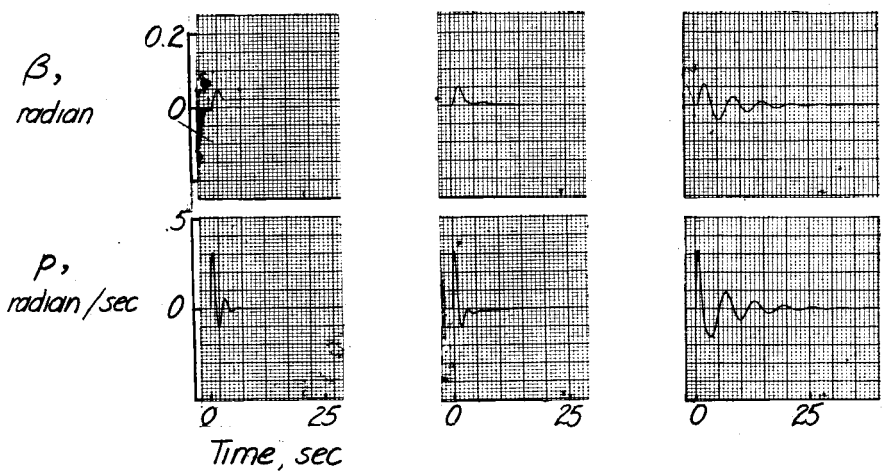

(a) Response to step e_{lat}. $\delta_e = 0^\circ$.

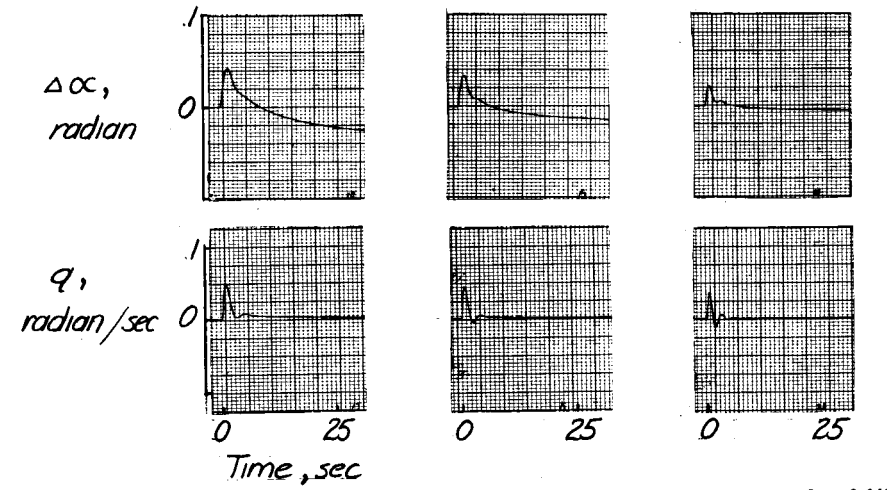

(b) Response to step e_{long}. $\delta_a = 0^\circ$.

Figure 8.- Open-loop response to step inputs of e_{long} and e_{lat}.

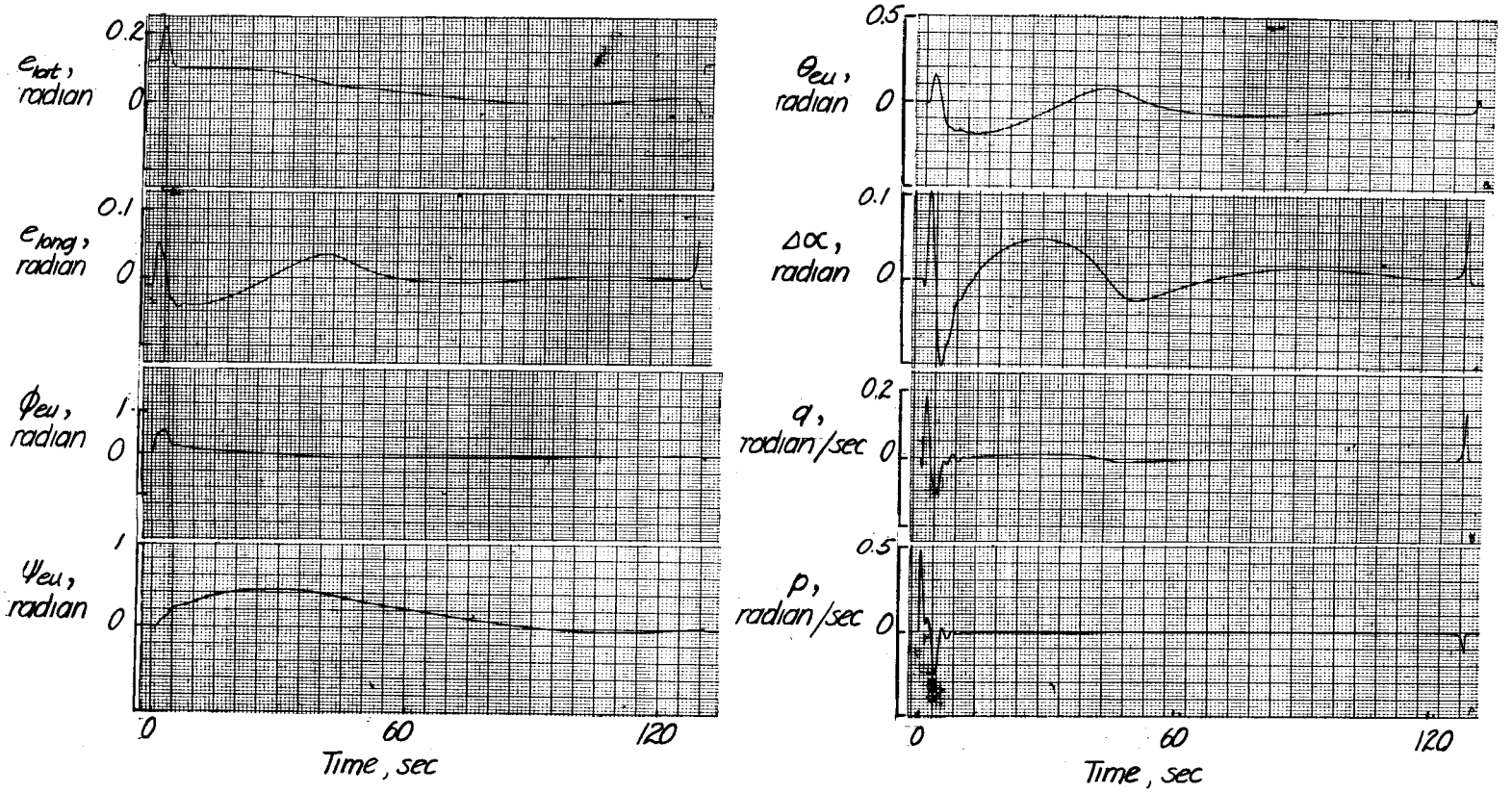

(a) $\delta_a = -6e_{lat} + 1\psi_{eu} + 2 \int p\, dt.$

Figure 9.- Typical case with no limit on e_{lat}. $\theta_{a,o} = 6.52^\circ$; $\theta_{e,o} = -3.14^\circ$; $\theta_{eu,o} = \psi_{eu,o} - \phi_{eu,o} = 0^\circ$; R = 5 miles;

$\delta_e = -8e_{long} + 1.5\theta_{eu} + 0.32q + 0.64 \int q\, dt.$

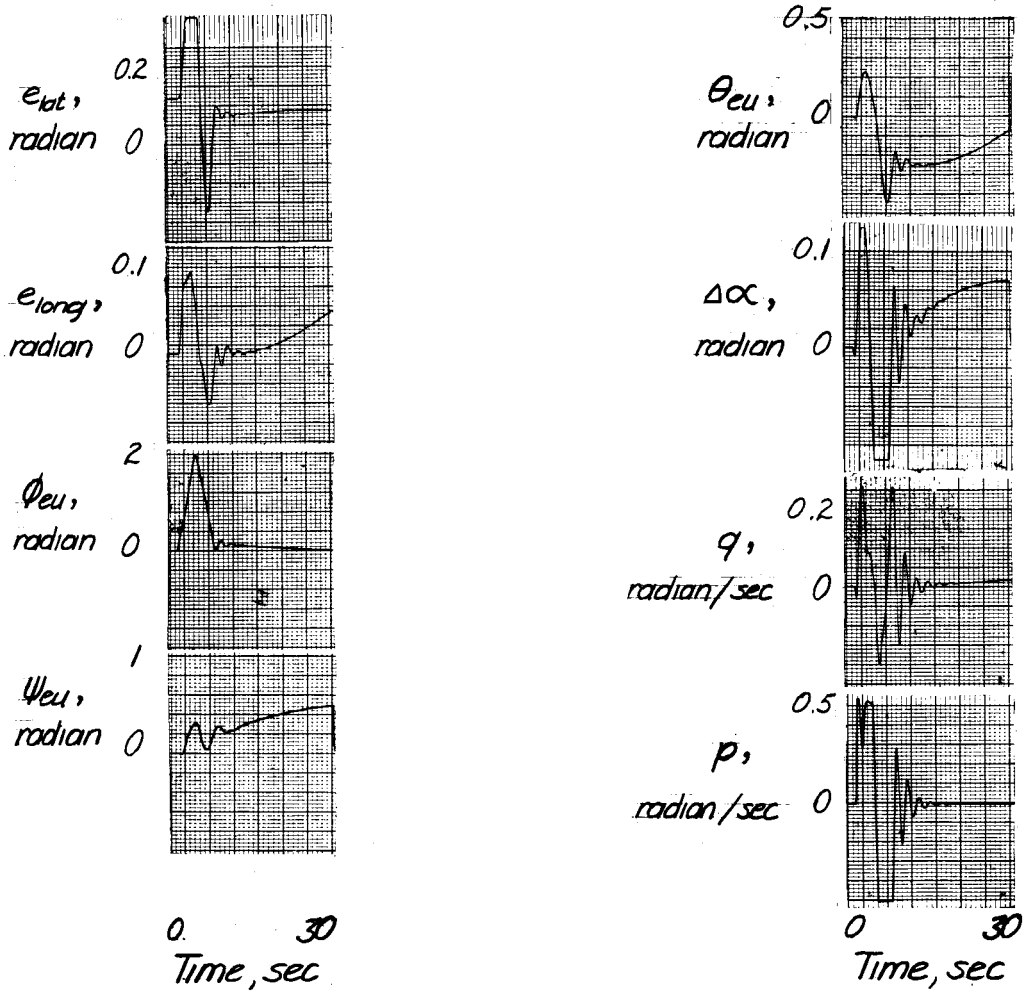

(b) $\delta_a = -8e_{lat} + 1\psi_{eu} + 2 \int p \, dt.$

Figure 9.- Concluded.

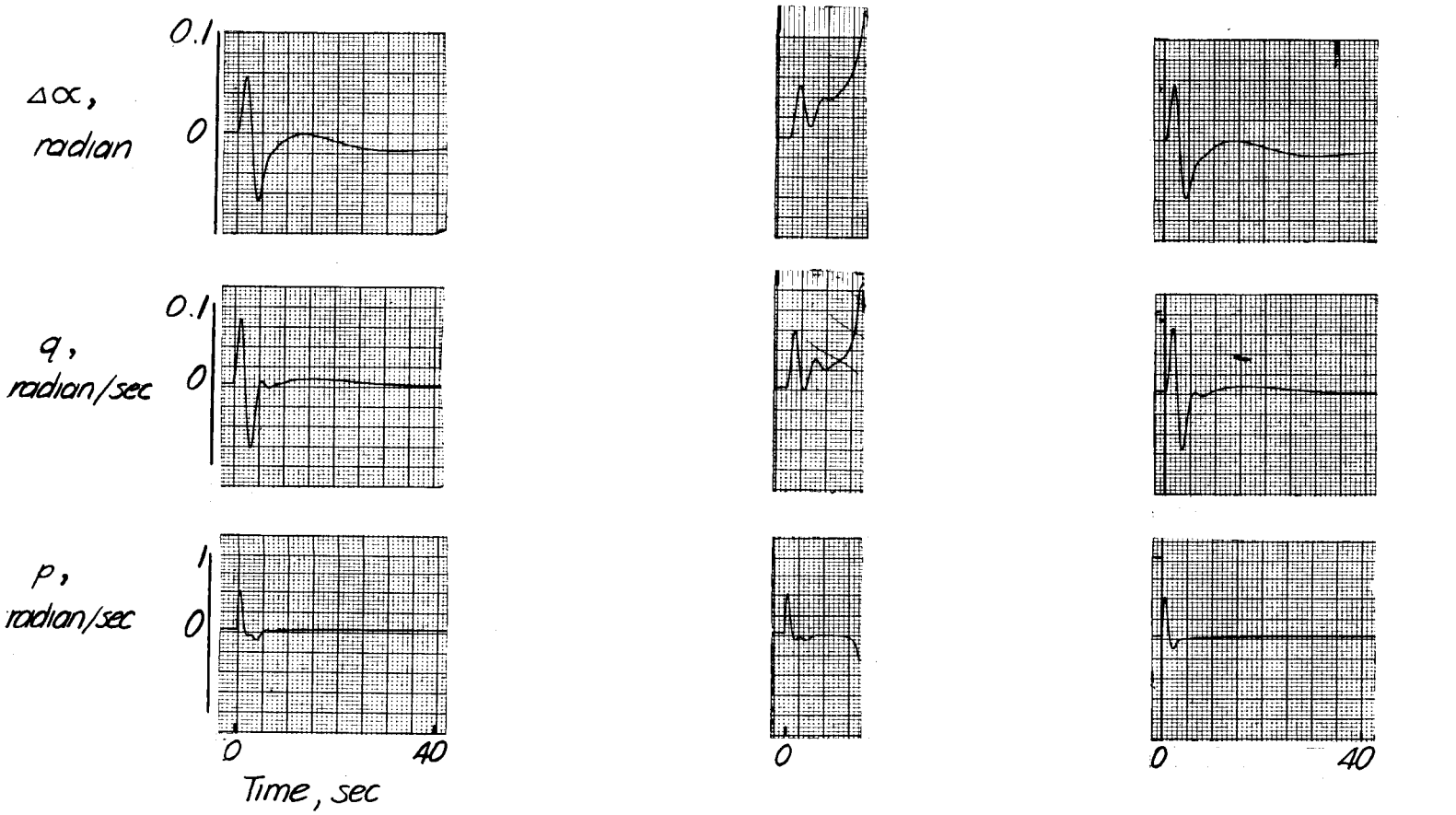

(a) $\delta_a = -6e_{lat} + 2\psi_{eu} + 2\int p\,dt;$

$\delta_e = -3e_{long} + 0.07\theta_{eu} + 0.32q + 0.64\int q\,dt.$

(b) $\delta_a = -6e_{lat} + 2\psi_{eu} + 2\int p\,dt;$

$\delta_e = -3\theta_{eu} - 3\int q\,dt + 0.07\int q\,dt + 0.32q + 0.64\int q\,dt.$

(c) $\delta_a = -6\theta_a - 6\int r\,dt + 2\int r\,dt + 2\int p\,dt;$

$\delta_e = -3e_{long} + 0.07\theta_{eu} + 0.32q + 0.64\int q\,dt.$

Figure 10.- Effect of change in attitude quantities. $\theta_{a,o} = 6.52^o$; $\theta_{e,o} = -2.21^o$; $\theta_{eu,o} = \psi_{eu,o} = \phi_{eu,o} = 0^o$; R = 5 miles.

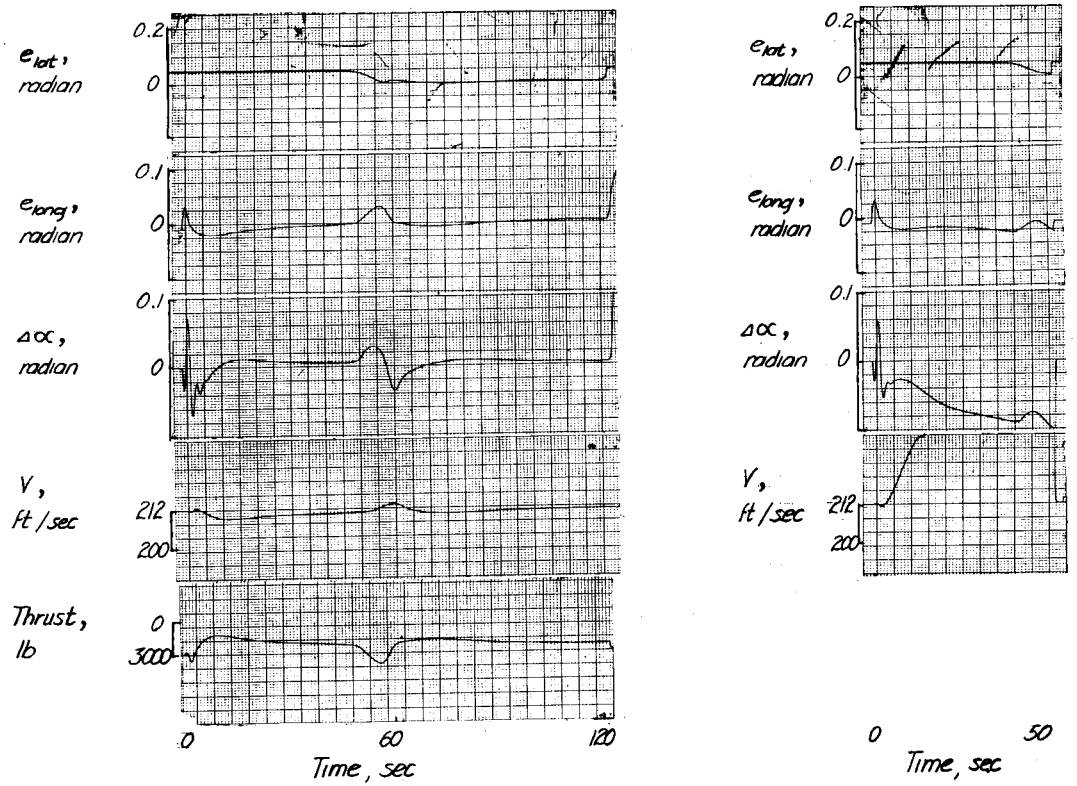

(a) $\Delta T = \left(14{,}800 \sin \theta_{eu} - 68\ \Delta V\right)\frac{1}{1 + s}$.

(b) $\Delta T = 0$.

Figure 11.- Effect of various airspeed controls. $\theta_{a,o} = 6.52^{\circ}$; $\theta_{e,o} = -3.14^{\circ}$; $\theta_{eu,o} = \psi_{eu,o} = \phi_{eu,o} = 0^{\circ}$; R = 5 miles; $\delta_a = -12e_{lat} + 1.75\psi_{eu} + 2\int p\ dt$; $\delta_e = -10e_{long} + 2.5\left(\theta_{eu} + 2.5^{\circ}\right) + 0.32q + 0.64\int q\ dt$.

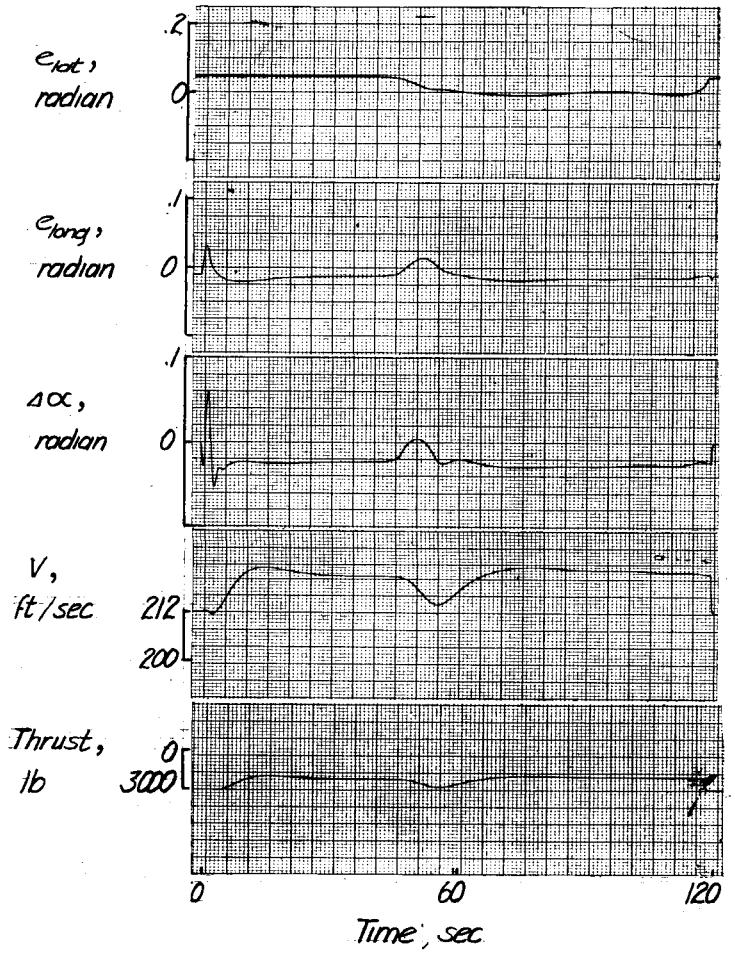

(c) $\Delta T = (-68\ \Delta V)\frac{1}{1+s}$.

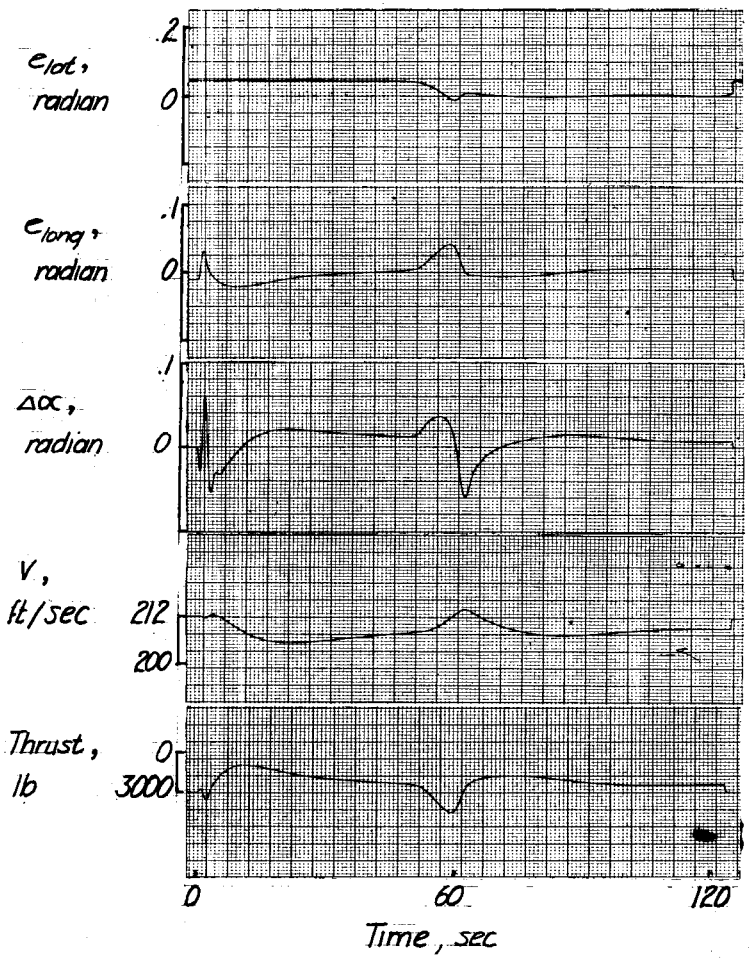

(d) $\Delta T = (14{,}800 \sin \theta_{eu})\frac{1}{1+s}$.

Figure 11.- Concluded.

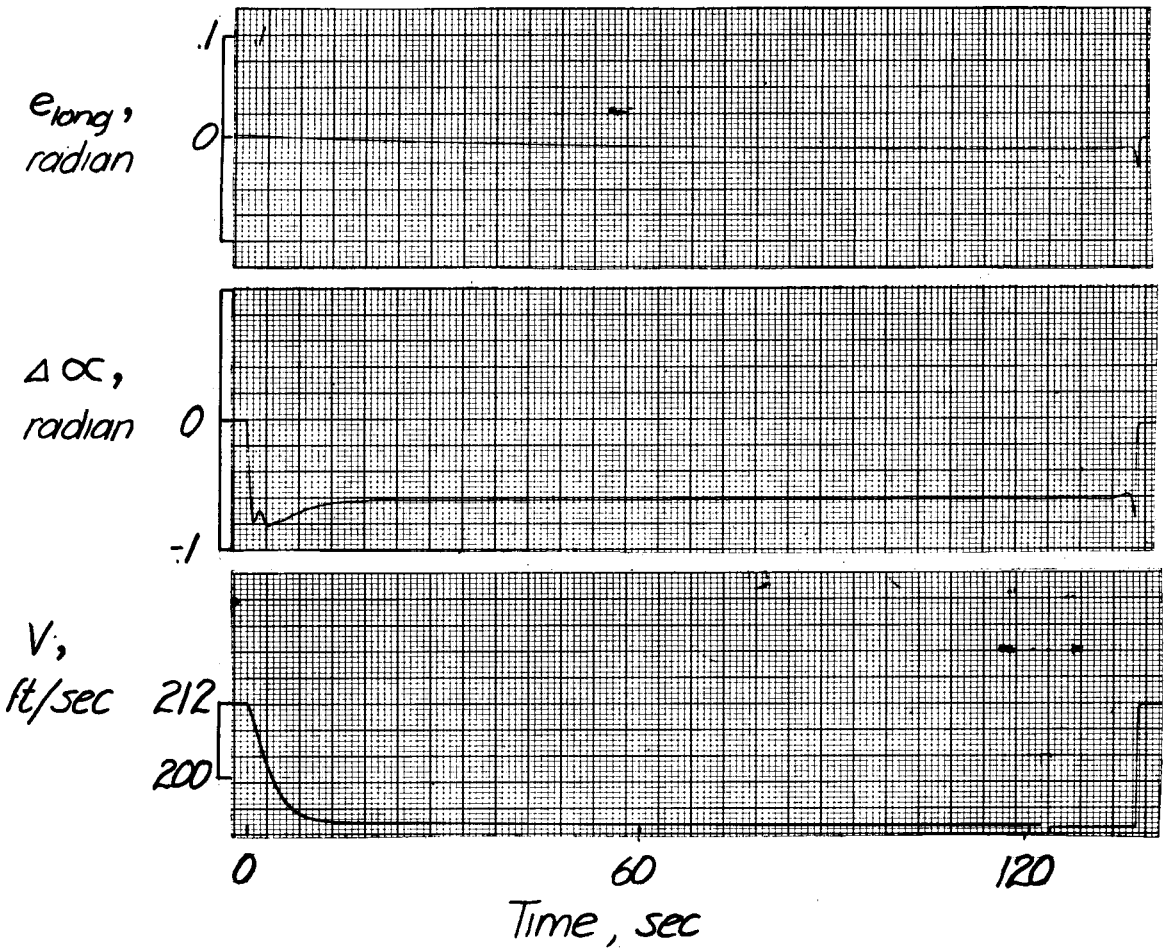

Figure 12.- Effect of flap deflection; $\theta_{a,o} = 0^\circ$; $\theta_{e,o} = 0^\circ$; $\theta_{eu,o} = -2.5^\circ$; $\psi_{eu,o} = 0^\circ$; $\phi_{eu,o} = 0^\circ$;

$\delta_a = -12e_{lat} + 1.75\psi_{eu} + 2\int p\,dt$; $\delta_e = -10e_{long} + 2.5(\theta_{eu} + 2.5^\circ) + 0.32q + 0.64\int q\,dt$;

$\Delta C_m = -0.05$; $\Delta C_Z = -0.4$; $\Delta C_X = -0.07$.

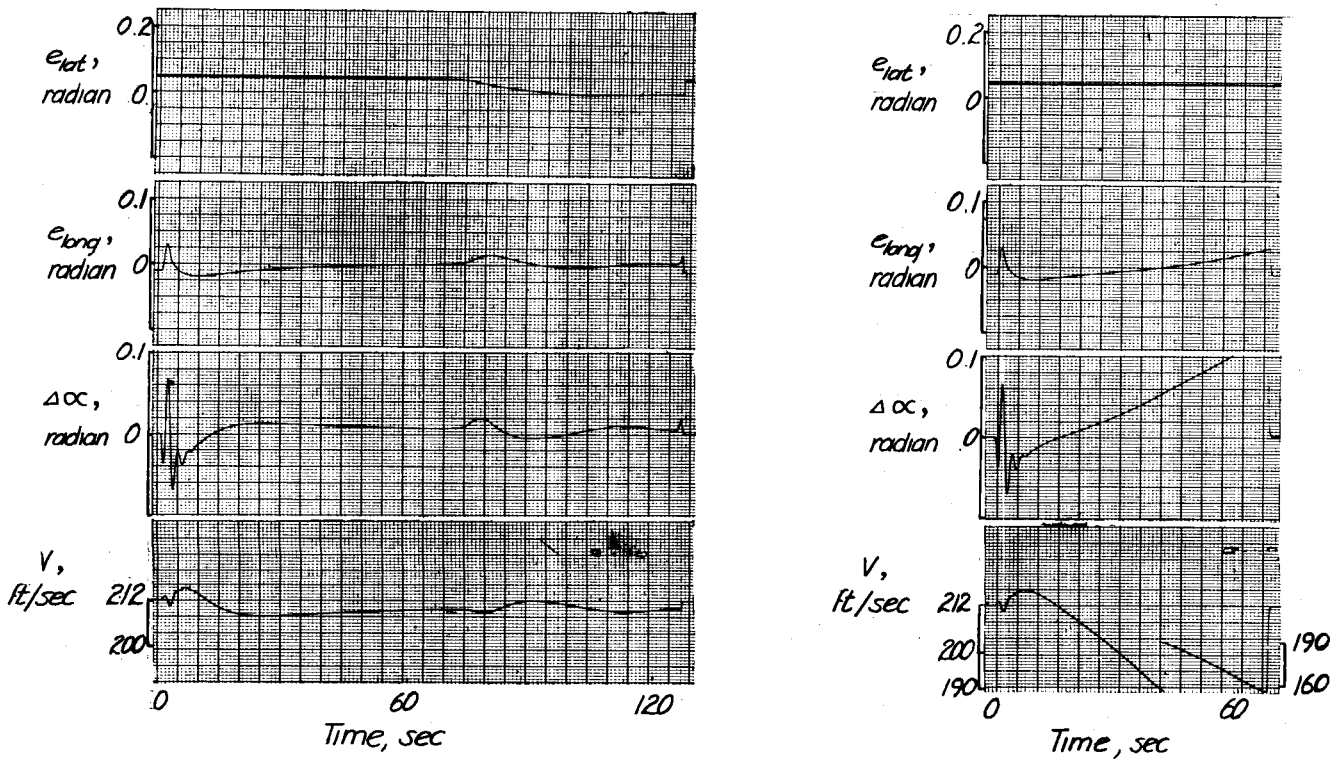

(a) $\Delta T = \left(14{,}800 \sin \theta_{eu} - 68\,\Delta V\right)\frac{1}{1+s}$.

(b) $\Delta T = \left(14{,}800 \sin \theta_{eu}\right)\frac{1}{1+s}$.

Figure 13.- Response with $C_{X_\alpha} = -0.63$. $\theta_{a,o} = 6.52^\circ$; $\theta_{e,o} = -3.14^\circ$; $\theta_{eu,o} = \psi_{eu,o} = \phi_{eu,o} = 0^\circ$;

$R = 5$ miles; $\delta_a = -12e_{lat} + 2\psi_{eu} + 2\int p\,dt$;

$\delta_e = -10e_{long} + 2.5\left(\theta_{eu} + 2.5^\circ\right) + 0.32q + 0.64\int q\,dt$.

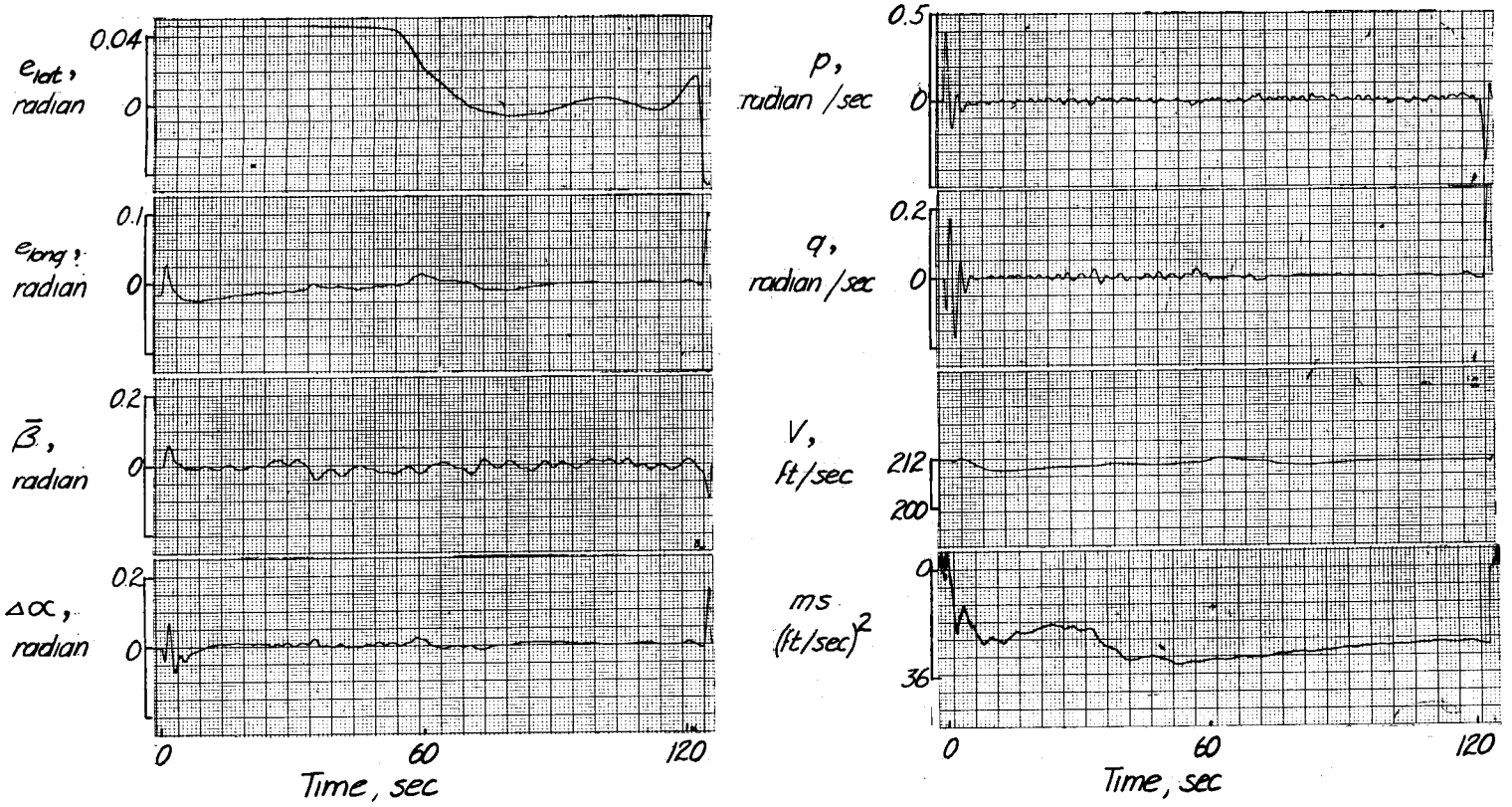

(a) Example 1, v_g rms = 6 ft/sec.

Figure 14.- Effect of random lateral gust disturbance. $\theta_{a,o} = 6.52^{\circ}$; $\theta_{e,o} = -3.14^{\circ}$; $\theta_{eu,o} = \Psi_{eu,o} = \phi_{eu,o} = 0^{\circ}$; R = 5 miles; $\delta_a = -12e_{lat} + 2\Psi_{eu} + 2\int p\,dt$; $\delta_e = -10e_{long} + 2.5(\theta_{eu} + 2.5^{\circ}) + 0.32q + 0.64\int q\,dt$; $\beta_t = \bar{\beta} + \beta q$.

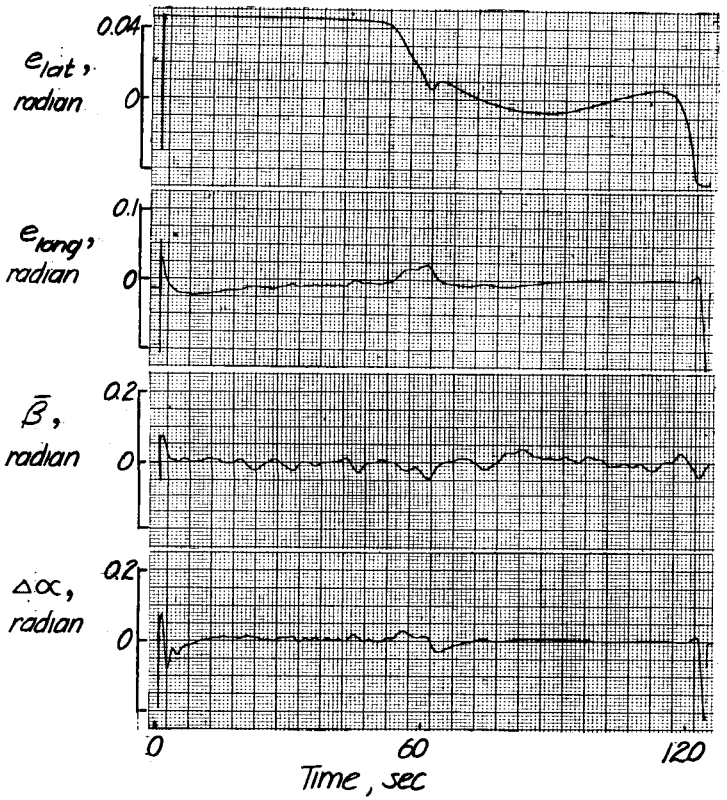

(b) Example 2, v_g rms = 6 ft/sec.

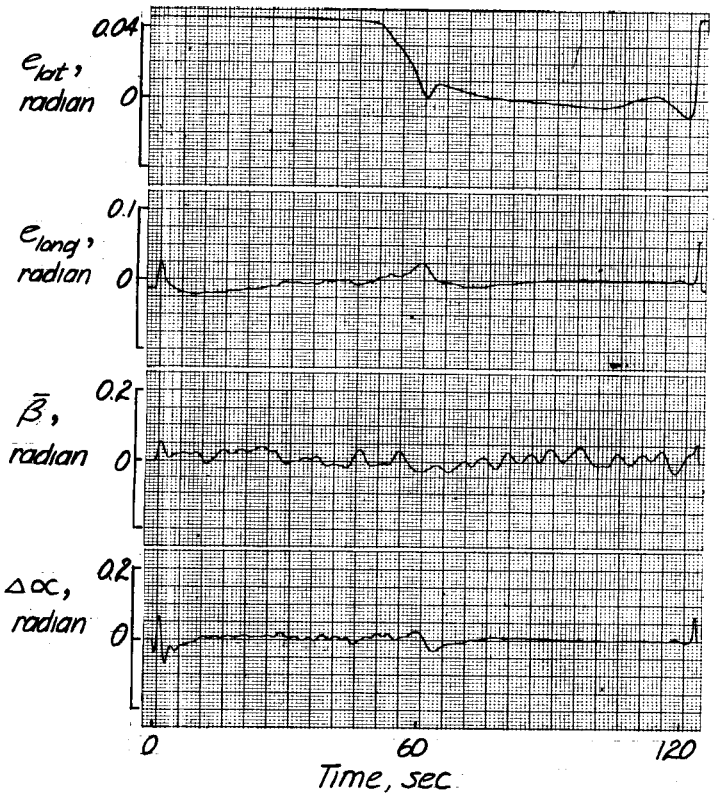

(c) Example 3, v_g rms = 6 ft/sec.

Figure 14.- Continued.

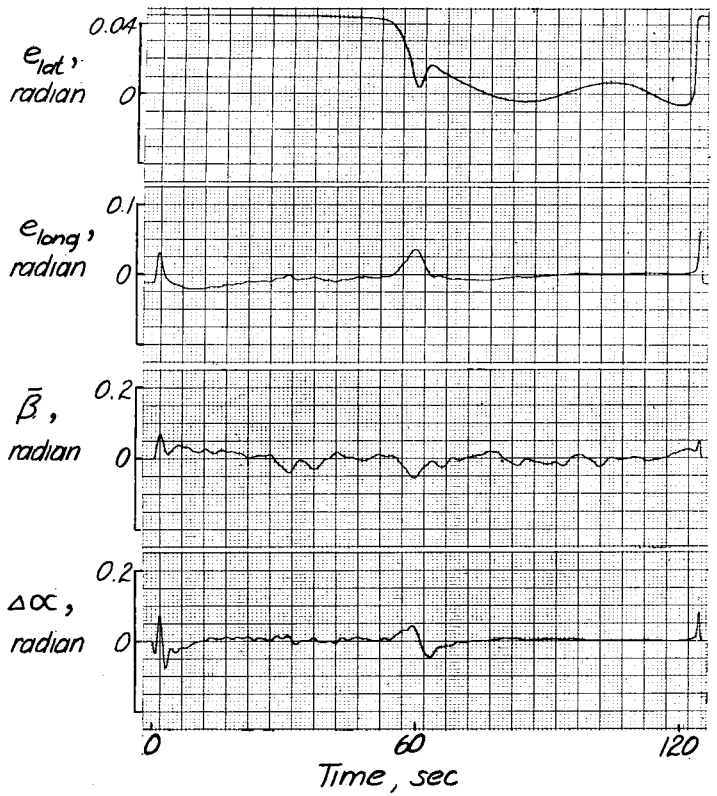

(d) Example 4, v_g rms = 6 ft/sec.

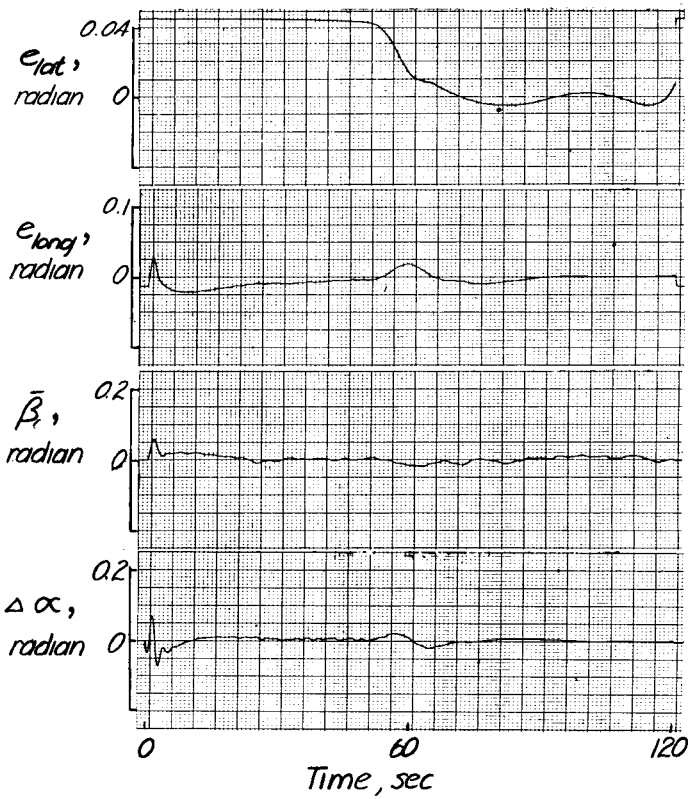

(e) Example 5, v_g rms = 3 ft/sec.

Figure 14.- Concluded.

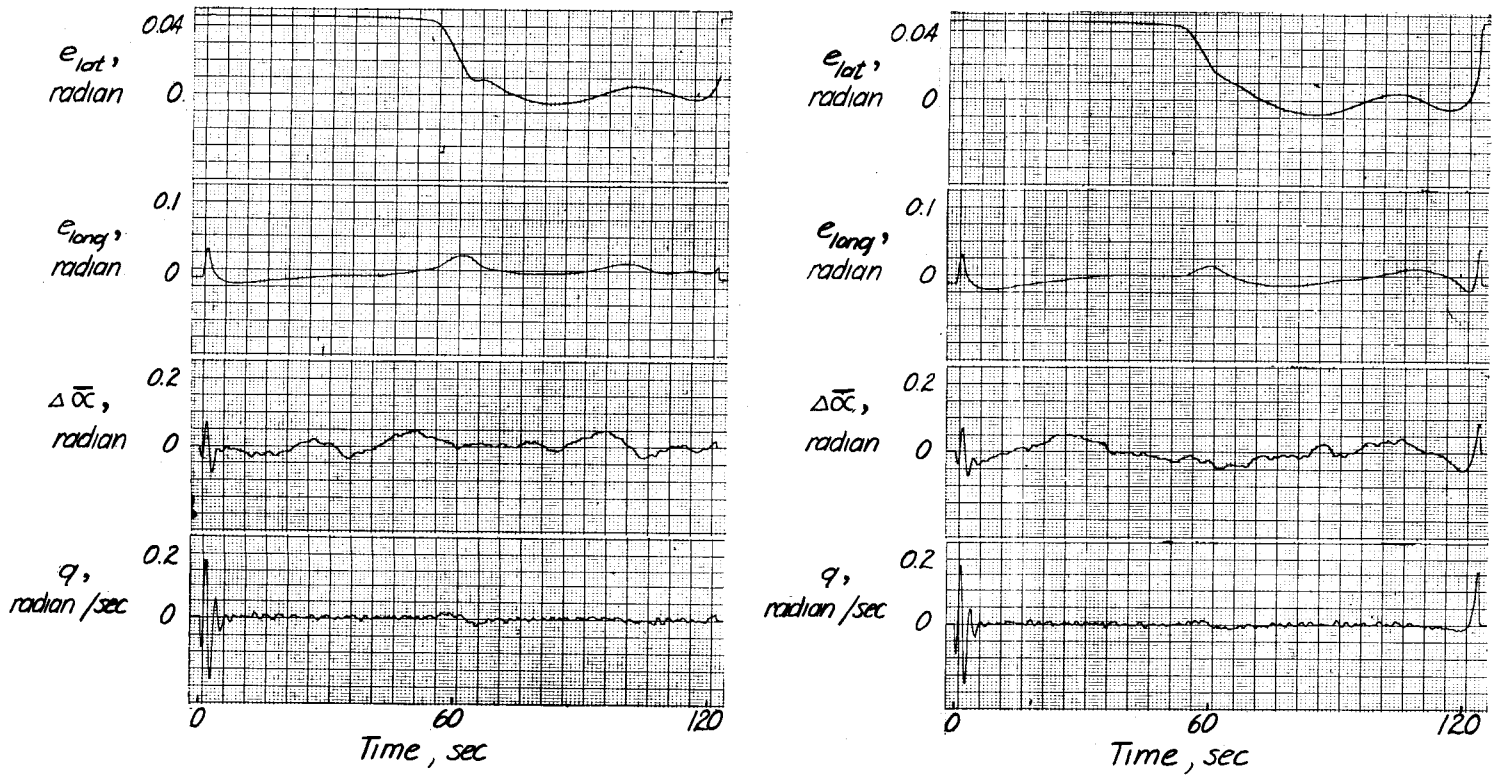

(a) Example 1.

(b) Example 2.

Figure 15.- Effect of random vertical gust disturbance. $\theta_{a,o} = 6.52^{\circ}$; $\theta_{e,o} = -3.14^{\circ}$; $\theta_{eu,o} = \psi_{eu,o} = \phi_{eu,o} = 0^{\circ}$; R = 5 miles; $\delta_a = -12e_{lat} + 2\psi_{eu} + 2\int p\,dt$; $\delta_e = -10e_{long} + 2.5(\theta_{eu} + 2.5^{\circ}) + 0.32q + 0.64\int q\,dt$; $\alpha_t = \bar{\alpha} + \alpha_g$; w_g rms = 6 ft/sec.

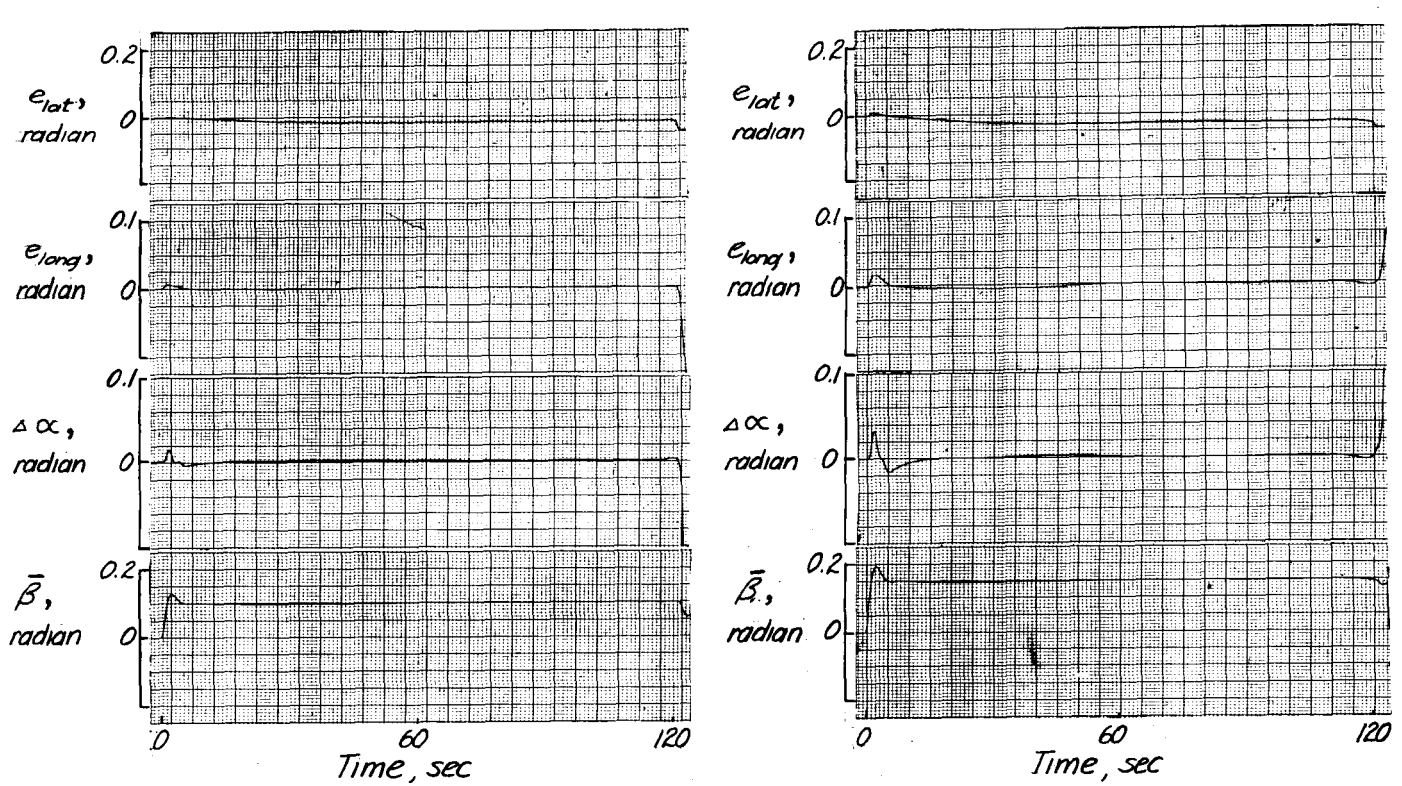

(a) β_g = -0.1 radian; $v_g \approx$ 20 ft/sec. (b) β_g = -0.15 radian; $v_g \approx$ 30 ft/sec.

Figure 16.- Effect of crosswind. $\theta_{a,o} = 0^o$; $\theta_{e,o} = 0^o$; $\theta_{eu,o} = -2.5^o$; $\psi_{eu,o} = \phi_{eu,o} = 0^o$;

R = 5 miles; $\delta_a = -12e_{lat} + 1.75\psi_{eu} + 2\int p\,dt$;

$\delta_e = -10e_{long} + 2.5(\theta_{eu} + 2.5^o) + 0.32q + 0.64\int q\,dt$; $\beta_t = \bar{\beta} + \beta_g$.

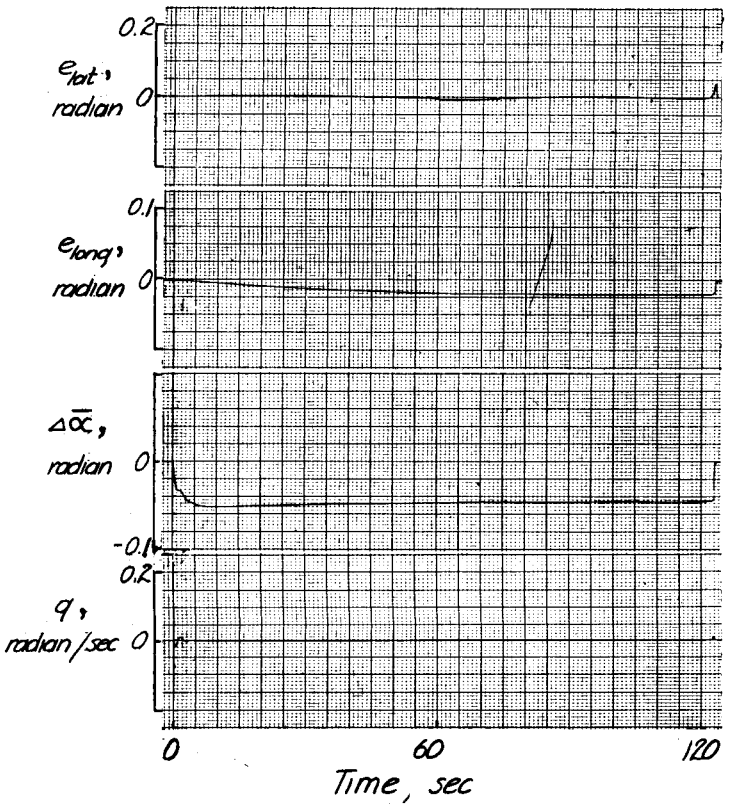

(a) $\Delta\alpha_g = 0.05$ radian; $w_g \approx 10$ ft/sec.

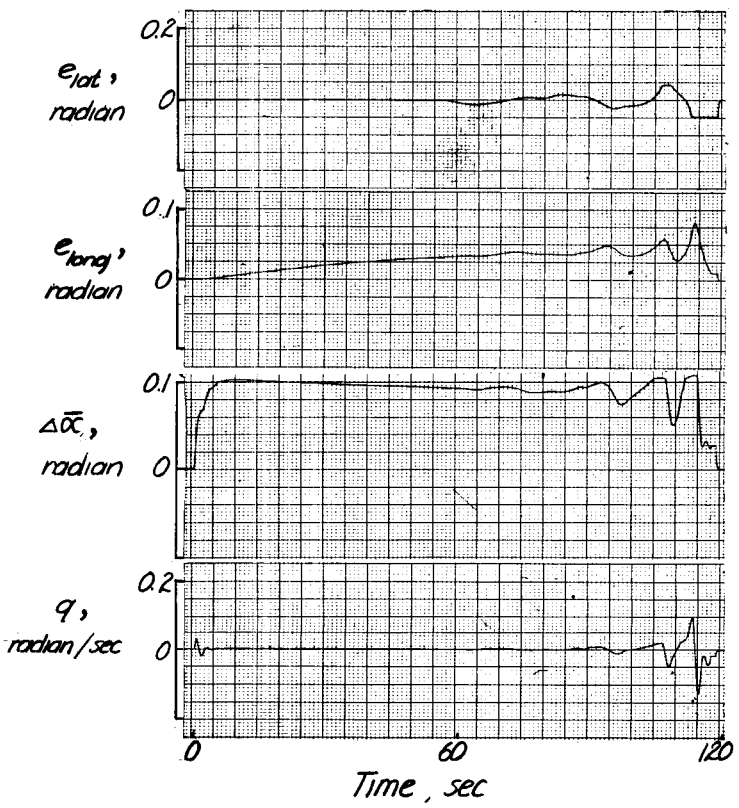

(b) $\Delta\alpha_g = -0.1$ radian; $w_g = -20$ ft/sec.

Figure 17.- Effect of vertical wind. $\theta_{a,o} = 0^\circ$; $\theta_{e,o} = 0^\circ$; $\theta_{eu,o} = -2.5^\circ$; $\psi_{eu,o} = \phi_{eu,o} = 0^\circ$;

$R = 5$ miles; $\delta_a = -12e_{lat} + 1.75\psi_{eu} + 2\int p\,dt$;

$\delta_e = -10e_{long} + 2.5(\theta_{eu} + 2.5^\circ) + 0.32q + 0.64\int q\,dt$; $\alpha_t = \bar{\alpha} + \alpha_g$.

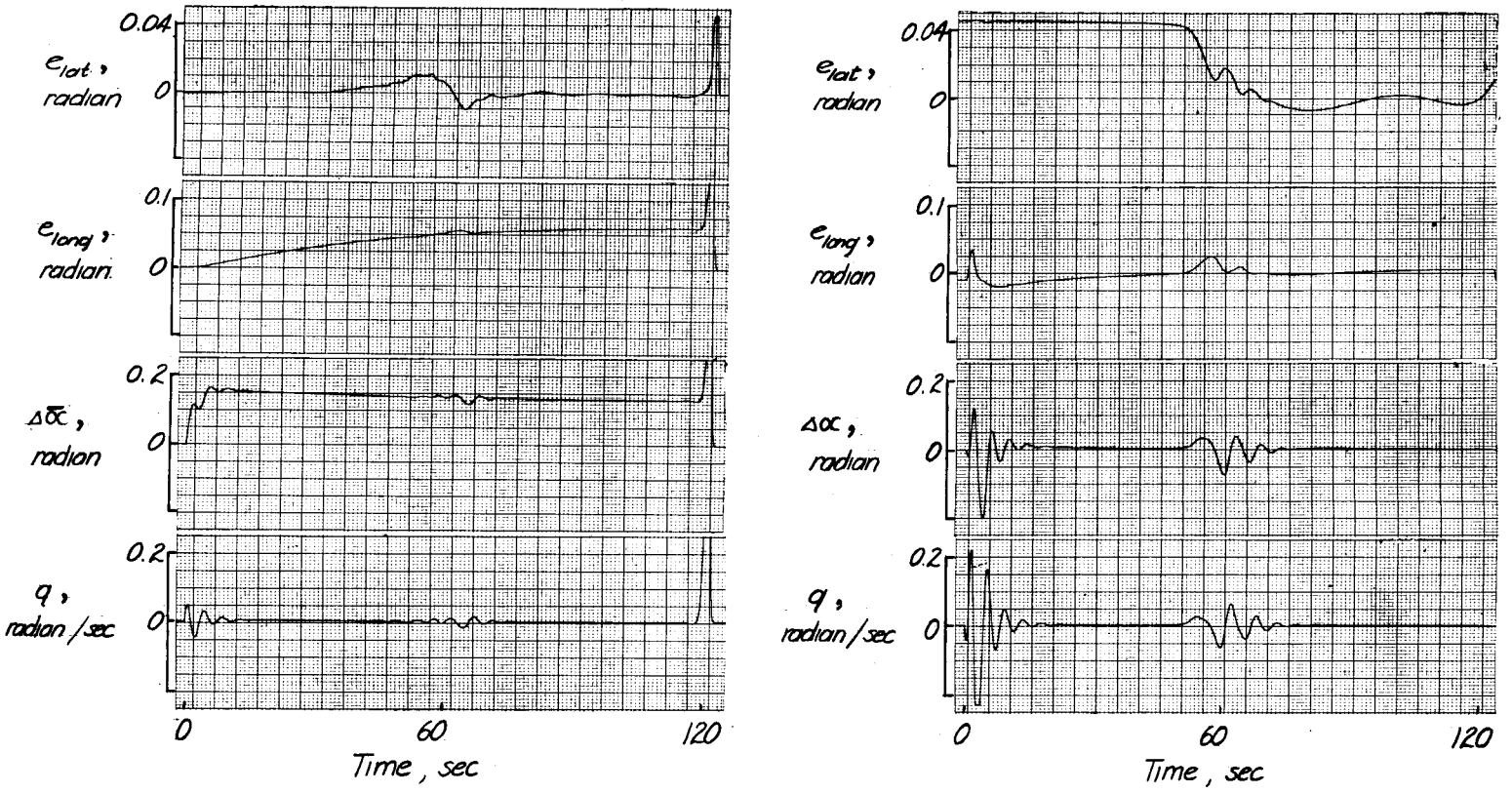

(a) $\theta_{e,o} = 0^\circ$; $\theta_{a,o} = 0^\circ$; $\theta_{eu,o} = -2.5^\circ$; $\psi_{eu,o} = \phi_{eu,o} = 0^\circ$; $\alpha_g = -0.15$ radian; $w_g = -30$ ft/sec.

(b) $\theta_{e,o} = 6.52^\circ$; $\theta_{a,o} = -3.14^\circ$; $\theta_{eu,o} = \psi_{eu,o} = \phi_{eu,o} = 0^\circ$.

Figure 18.- Effect of the addition of a first-order lag to the longitudinal damping.

$\delta_a = -12e_{lat} + 2\psi_{eu} + 2\int p\,dt$; $\delta_e = -10e_{long} + 2.5(\theta_{eu} + 2.5^\circ)\frac{1}{1+2s} + 0.32q + 0.64\int q\,dt$; $R = 5$ miles.

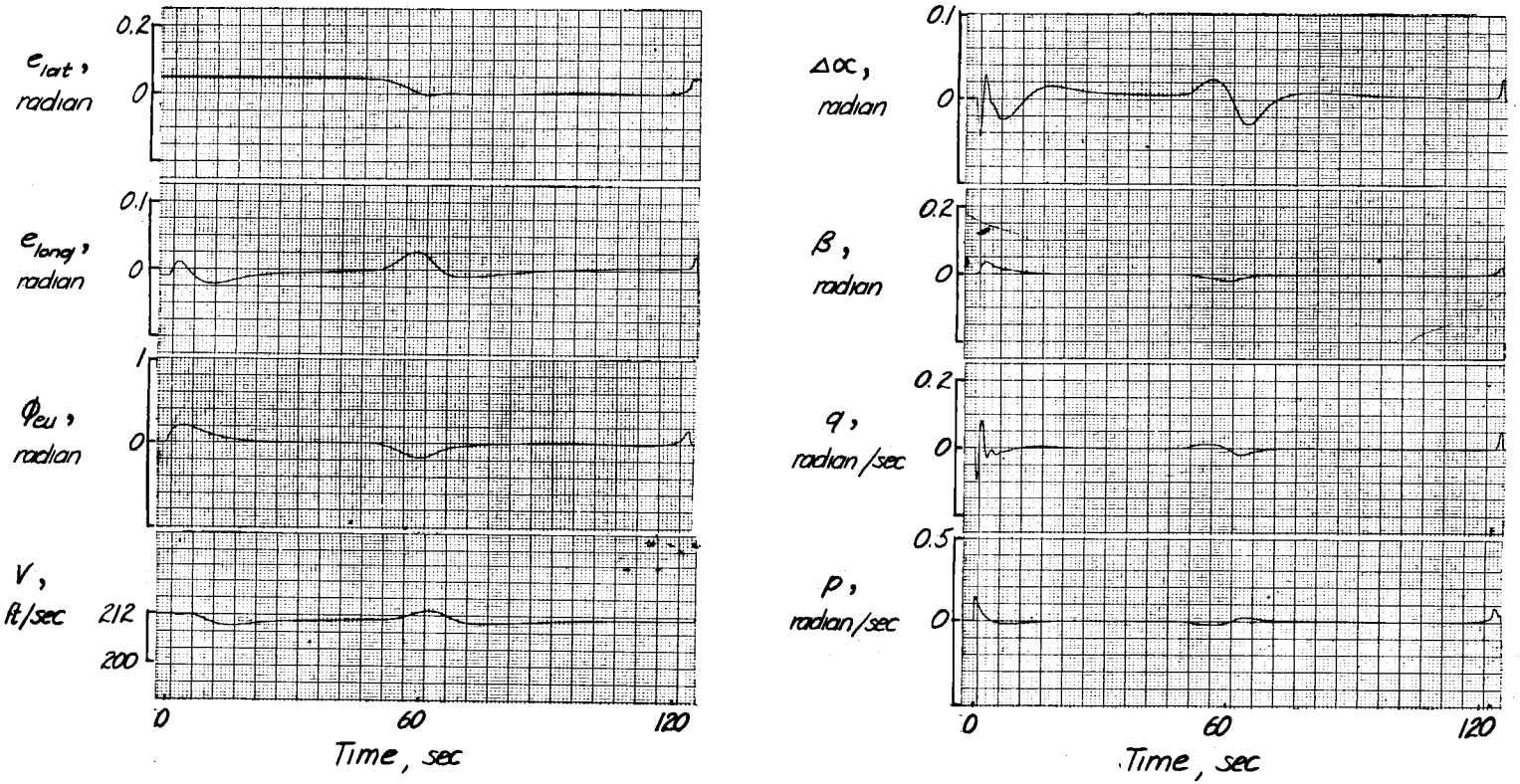

Figure 19.- Effect of the addition of roll damping. $\theta_{a,o} = 6.52^{\circ}$; $\theta_{e,o} = -3.14^{\circ}$; $\theta_{eu,o} = \psi_{eu,o} = \phi_{eu,o} = 0^{\circ}$; R = 5 miles; $\delta_a = -12e_{lat} + 1.75\psi_{eu} + 2\int p\,dt + 0.7\,p$; $\delta_e = -10e_{long} + 2.5(\theta_{eu} + 2.5^{\circ}) + 0.32q + 0.64\int q\,dt$.

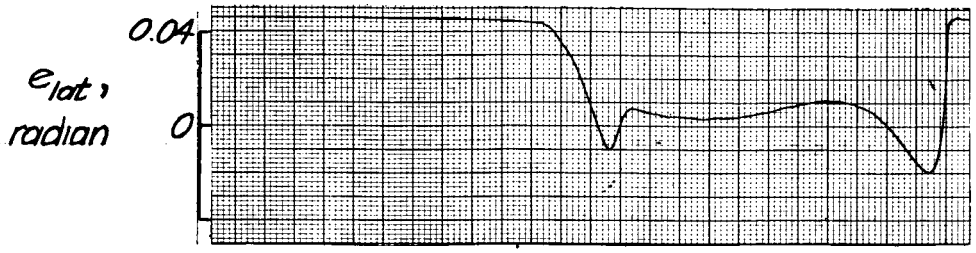

(a) Example 1

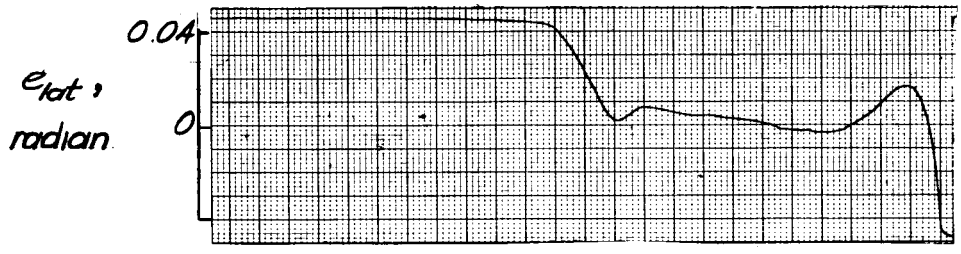

(b) Example 2

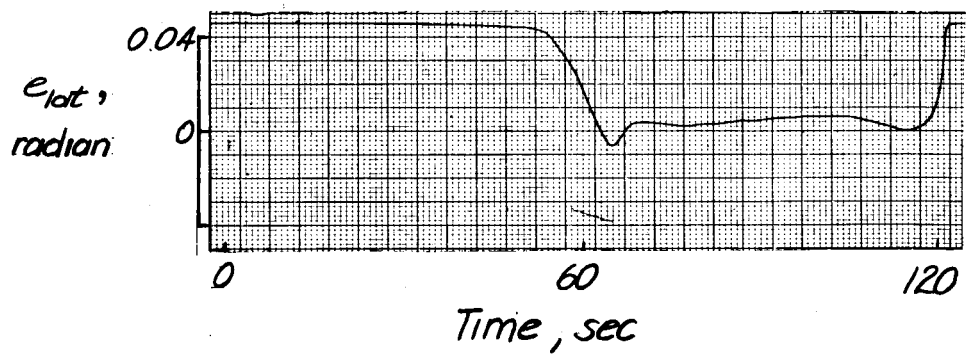

(c) Example 3

Figure 20.- Effect of random lateral gust disturbances in combination with additional roll damping. $\theta_{a,o} = 6.52^{\circ}$; $\theta_{e,o} = -3.14^{\circ}$; $\theta_{eu,o} = \psi_{eu,o} = \phi_{eu,o} = 0^{\circ}$; R = 5 miles; $\beta_t = \beta_o + \beta_g$; β_g rms = 6 ft/sec; $\delta_a = -12e_{lat} + 2\psi_{eu} + 2\int p\,dt + 0.7p$; $\delta_e = -10e_{long} + 2.5(\theta_{eu} + 2.5^{\circ}) + 0.32q + 0.64\int q\,dt$; $\beta_t = \bar{\beta} + \beta_g$.

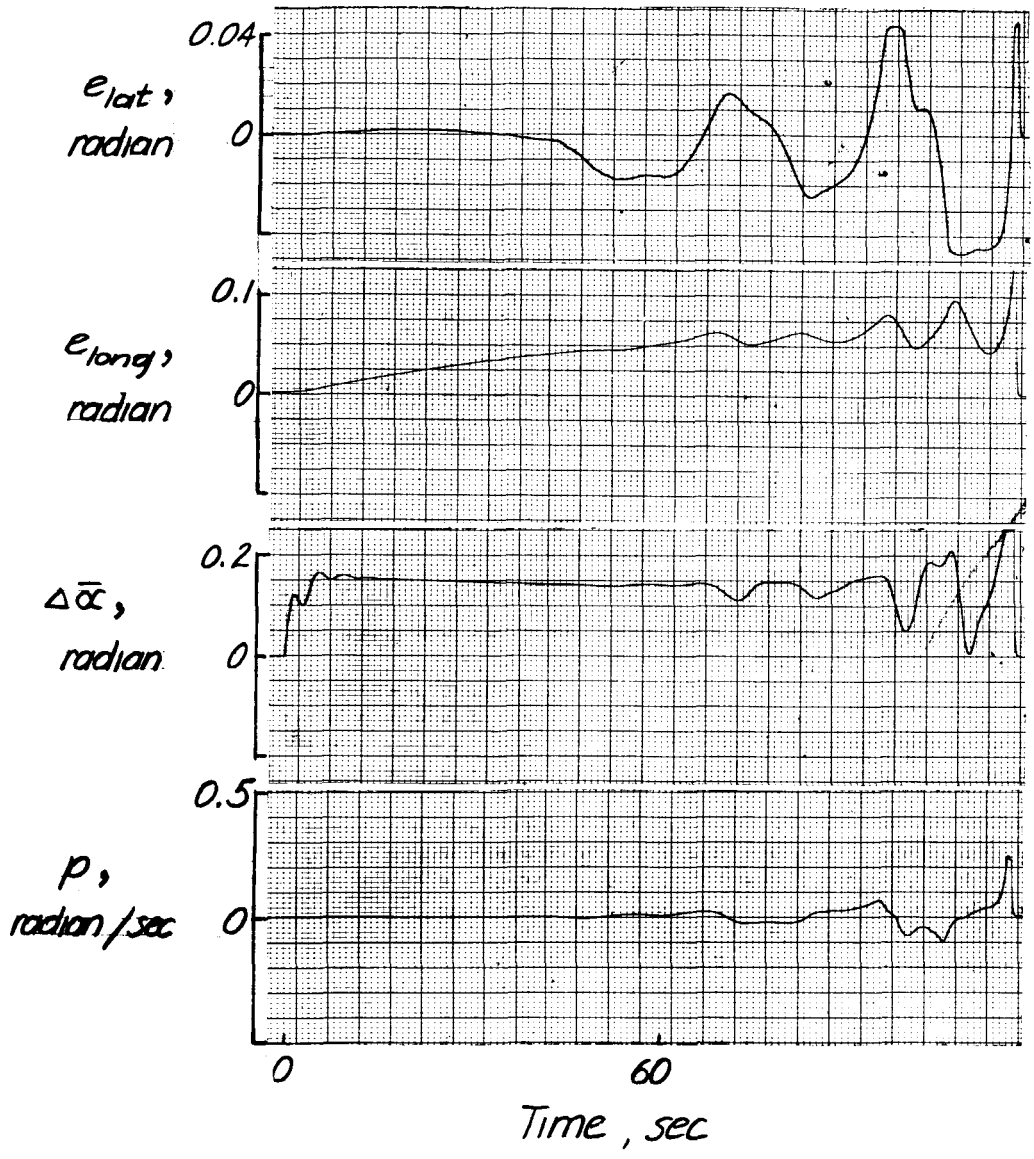

Figure 21.- Effect of combining additional roll damping and a first-order lag on longitudinal damping in the presence of a vertical wind. $\theta_{a,o} = 0^\circ$; $\theta_{e,o} = 0^\circ$; $\theta_{eu,o} = -2.5^\circ$; $\psi_{eu,o} = \phi_{eu,o} = 0^\circ$; R = 5 miles;

$$\delta_a = -12e_{lat} + 2\psi_{eu} + 2\int p\,dt + 0.7p;$$

$$\delta_e = -10e_{long} + 2.5(\theta_{eu} + 2.5^\circ)\frac{1}{1+2s} + 0.32q + 0.64\int q\,dt;$$

$\alpha_t = \bar{\alpha} + \alpha_g$; $\Delta\alpha_g = -0.15$ radian; $w_g = -30$ ft/sec.

NASA - Langley Field, Va. L-493

L-493